Deanship of Graduate Studies

Al-Quds University

The effect of Embedded ZnO and Au Nanoparticles on Schottky Diode Characteristics

Mary Anton Hanna Mousallam

M.Sc. Thesis

Jerusalem

2022\1443

The effect of Embedded ZnO and Au Nanoparticles on Schottky Diodes Characteristics

Prepared by:

Mary Anton Hanna Mousallam

B.Sc. Mathematics, Bethlehem University, Palestine

Supervisors:

Dr. Jamal Ghabboun	Dr. Hazem Doufesh
Physics Department	Physics Department
Bethlehem University	Al-Quds University

"A thesis submitted to the Faculty of Science and Technology, Al-Quds University in Partial Fulfilment of the Requirements for the Degree of Master of Science in Physics"

2022\1443

Al-Quds University

Deanship of Graduate Studies

Physics Department

Thesis Approval

The effect of Embedded ZnO and Au Nanoparticles on Schottky Diode Characteristics

Prepared by: Mary Anton Hanna Mousallam

Registration No.: 21620039

Supervisor: Dr. Jamal Ghabboun

Co-Supervisor: Dr. Hazem Doufesh

Master thesis submitted and accepted, Date: 6 / 8 / 2020

The names and signatures of the examining committee members are as follows:

1. Supervisor: Dr. Jamal Ghabboun Signature
2. Co-Supervisor: Dr. Hazem Doufesh Signature
3. Internal Examiner: Dr. Rushdi Kittaneh Signature
4. External Examiner: Dr. Ishaq Musa Signature

Jerusalem – Palestine

2022/1443

Declaration:

I certify that this thesis submitted for the degree of master is the result of my own research, except where otherwise acknowledged, and that this thesis (or any part of the same) has not been submitted for a higher degree to any other university or institution.

Signed: 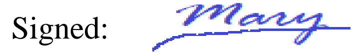

Mary Anton Hanna Mousallam

Date: 6 / 8 /2022

Dedication

I am thankful to all those who played a great role in motivating me throughout my journey of this thesis paper.

Thereby, I dedicate this to my beloved family,

My father and my mother,

My brothers,

My friends,

And my teachers.

Acknowledgment

I would like to seize this opportunity to convey my sincere and heartfelt gratitude first to my supervisor, Dr. Jamal Ghabboun, without whom my thesis would never have taken its current form. I am greatly indebted to him for advising and guiding me during the course of my research and for giving me the chance to use all available and purchased equipment and materials in the Physics Laboratory at Bethlehem University. I also extend my sincere thanks to my supervisor Dr. Hazem Doufesh for his encouragement, support and valuable advice to improving this thesis.

It is an honour for me to thank all employees at Al-Quds University, for facilitating their FTIR device and laboratories in order to complete our study. Many thanks to Dr. Ahmad Jabareen, head of the Materials engineering department, and to Mrs. Maryam Haroun from the Nano-Lab Research Laboratory in the Materials Engineering department for their assistance in using their equipment.

I would like to thank especially Engineer Mr. Nader Adawi for providing me with the technical help with experiments and data acquisition.

Warm thanks go to the Dean of research at Bethlehem University, prof. Jamil Khader and for the Palestinian Ministry of Higher education for their funding of the materials that have been used in this research study.

I would also like to express my gratitude for all employees and workers in Bethlehem University laboratories, both Physics and Chemistry, for Dr. Michel Hanania, Dean of science and head of the Chemistry department and Mrs Firial Bannoura for allowing the use of the chemistry lab and for their valuable help in preparation of the chemical solutions. Also I would like to express my gratitude for Mr. Ahmad Atiyha for his help at the Physics laboratory at Bethlehem University.

I am deeply indebted to Dr. Sawsan Abu-Sharkh for everything that she had taught me throughout my journey.

Finally, I am deeply grateful for my parents, my brothers, and my friends for their constant support and uplifting my spirits during difficult times.

List of Abbreviations and Symbols

ZnO	Zinc Oxide
Au	Gold
Ag	Silver
Si	Silicon
NPs	Nanoparticles
E_F	Fermi level
E_{F_M}	Fermi level in Metals
E_{F_S}	Fermi level in Semiconductors
E_g	Energy band gap
E_C	Energy lever at the bottom of the conduction band
E_V	Energy level at the top of the valence band
MS	Metal-semiconductor
SBH	Schottky Barrier Height
Φ	Work function
Φ_B	Zero bias Barrier Height
Φ_M	Work function of the Metal
Φ_S	Work function of the Semiconductor
χ	Electron affinity
n	Concentration of the donors
e	Elementary charge (proton)
ϵ	Dielectric constant
ϵ_0	Dielectric permittivity of Vacuum
x_b	Width of the depletion region at the PN junction
q	Charge of electron
I	Current
I_o	Reverse saturation current
DC	Direct current
AC	Alternating current
n	Ideality factor
k	Boltzmann constant
A*	Richardson constant
T	Temperature
$I_\circ$	Reverse saturation current
V	Voltage
V_A	Applied bias voltage
DW	Distilled water
IV	Current-Voltage
R_c	Contact resistance
R_S	Series resistance
R_{Sh}	Shunt resistance
θ	Contact angle
γ_l	Liquid surface tension
γ_s	Solid surface tension
γ_{sl}	Solid-Liquid surface tension
A	Absorbance
T	Transmittance
FTIR	Fourier transform infrared spectroscopy
rpm	Round per minute

Abstract

Optoelectronic devices and their optimization, is highly dependent on the accuracy of determining the electrical properties of such devices. In the last decade, studies for next generation electronics have considered organic components and nanoparticles to be inserted in rectifiers for their forward and facile patterning, their adjustable structure, lightweight, and flexibility, with the focus on integrating them in circuits which requires developing new ways to control the interference between semiconductors and metals as in the case of Schottky diodes.

The effect of interface modification with nanoparticles (NP) of a Metal/Semiconductor (MS) Schottky device will be discussed through parameters analysis such as Schottky Barrier Height (SBH) and ideality factor. Nanoparticles will be deposited on the surface of a semiconductor using controlled spin coating, followed by thermal evaporation for metal deposition to form the Schottky diode. Electrical characterization will be mainly carried out through current-voltage (I-V) characteristics. The modified surface of semiconductor with nanoparticles will be characterized to study the dependence of the conductivity behaviour of the metal/Nanoparticles/semiconductor device on the topography of the deposited nanoparticles on the semiconductor.

The effect of nanoparticles on the conductivity is studied using the current-voltage output curve characteristics both in the forward (positive voltage) and reverse (negative voltage) biases, and a diode model is used for fitting the data, hence information about Schottky Barrier Height (SBH) and ideality factor could be estimated in addition to the series resistance (R_s) and Shunt resistance (R_{sh}). Moreover, the effect of illumination on current-voltage characteristic have been carried out with samples tested in dark and light to study the effect of light induced current (Photocurrent).

A self-developed contact angle measurement method, was used to prove that the surface of the semiconductor was modified upon deposition of nanoparticles. Prior to process of the diode preparation, the surface of the semiconductor has been chemically etched to use a

clean surface of all impurities and defects. Additionally, I put into service Fourier-transform infrared spectroscopy (FTIR) to identify the deposited nanoparticles placed on the surface of the semiconductor.

N-type Silicon (Si) was used as the semiconductor while Silver (Ag) and Gold (Au) were used as metals. ZnO and Gold nanoparticles were used as the embedded layers at the interface to modify the semiconductor Schottky diode. The following samples were used to complete and conclude this type of research, Ag/Si, Au/Si, Ag/ZnO(NP)/Si and Ag/Au(NP)/Si, Au/ZnO(NP)/Si and Au/Au(NP)/Si.

Contact angle measurement showed that the surface has been modified after the NP insertion by turning from hydrophobic to hydrophilic behaviour or even the inverse. FTIR showed the appearance of Gold and ZnO nanoparticles on the modified Silicon substrate.

The extracted SBH from I-V curves showed an acceptable range of 0.2V-0.8V for all devices. The highest was for the etched Ag/Si device. Ideality factor for Schottky diodes was found to be 1 for all devices. R_s and R_{sh} showed an increase upon nanoparticles insertion in the Schottky device.

I-V characteristics were used to study light effect on Schottky devices with nanoparticles and it shows a decrease of barrier height with a significant decrease in shunt and series resistance.

أثر تضمين جزيئات النانو من نوعي أكسيد الزينك والذهب في خصائص الصمام الثنائي (ديود) شوتكي

اسم المشرف: الدكتور جمال غبون

اسم المشرف المساعد: الدكتور حازم دوفش

اسم الطالبة: ميري أنطون حنّا مسلّم

ملخص

الكهرو ضوئيات وتحسينها الى أفضل حد ممكن، يعتمد بشكل كبير على دقة تحديد الخصائص الالكترونية لأجهزتها. ففي العقد الأخير، أصبحت دراسة الجيل الجديد من الالكترونيات تأخذ بعين الاعتبار المكونات العضوية والجزيئات على مقياس النانو، واضافتها الى المقومات الالكترونية نظراً لسهولة أساليب تصميمها المباشرة، وتركيبها القابل للتعديل، وكتلتها الخفيفة ومرونتها، مع التركيز على دمجها في دارات تتطلب تطوير أساليب جديدة في التحكم بالسطح البيني للشبه موصلات والفلزات في حالة الصمام الثنائي (ديود) الشوتكي.

في هذه الدراسة قامت الباحثة بمناقشة أثر تعديل السطح البيني بجزيئات النانو لديود الشوتكي المكون من الفلز وشبه موصل، وذلك من خلال تحليل معامل ارتفاع حاجز الشوتكي، وعامل المثالية، عن طريق إضافة جزيئات النانو على سطح شبه الموصل باستخدام طريقة الطلاء الدوراني، متبوعاً بالتسامي الحراري للفلز لتشكيل ديود الشوتكي، ووصفت الخصائص الالكترونية من خلال عمل قياسات التيار-الجهد، وتحديد خصائص سطح شبه الموصل المعدّل بوجود جزيئات النانو، وذلك لدراسة مدى اعتماد التوصيل الكهربائي للأجهزة المكونة من (الفلز- جزيئات النانو- شبه الموصل) على تضاريس جزيئات النانو التي تغطي سطح شبه الموصل.

لدراسة أثر جزيئات النانو على التوصيل تم وصف منحنى التيار والجهد في حالتي تزويد الدارة بالجهد الموجب (أمامي) والجهد السالب (الخلفي)، واستخدام نموذج الصمام الثنائي (الديود) لتركيب البيانات واستخراج المعاملات مثل ارتفاع حاجز شوتكي، والمعامل المثالي، والمقاومة على التوالي والمقاومة المجزئة للتيار الكهربائي. كما وتم عمل قياس تيار- جهد بوجود اضاءة من اجل تفسير التيار الحثي.

من ناحية أخرى، تم تطوير آلية لقياس زاوية الاتصال لإثبات التعديل على السطح عند وضع جزيئات النانو عليه، مع العلم أن سطح شبه الموصل تم معالجته من خلال محلول كيميائي للتخلص من الشوائب والعيوب. وذلك بالاستعانة بالتحليل الطيفي (فورييه) FTIR، لتحديد وتأكيد نوعية جزيئات النانو الموجودة على سطح شبه الموصل.

علاوة على ذلك، قامت الباحثة باستخدام شبه الموصل السيليكون، نوع n، واعتماد الفلزات من نوع الذهب والفضة، أما جزئيات النانو المعتمدة في الدراسة كانت أكسيد الزينك والذهب ليتم تضمينها على شكل طبقات على السطح البيني لديود الشوتكي.

العينات التالية المستخدمة لاستكمال هذه الدراسة والخروج منها بالاستنتاجات هي:

Ag/Si, Au/Si, Ag/ZnO(NP)/Si, Ag/Au(NP)/Si, Au/ZnO(NP)/Si, Au/Au(NP)/Si.

أظهرت الدراسة أن قياس زاوية الاتصال أكد حدوث تعديلات على السطح نتيجة المواد الكيميائية واضافة جزيئات النانو، حيث تحول السطح من كاره للماء الى سطح محب للماء، كما وأظهرت نتائج التحليل الطيفي (فورييه) ظهور جزيئات الذهب وأكسيد الزينك على سطح السيليكون المعدّل كيميائياً، بالإضافة إلى أن قيم حاجز ديود الشوتكي المستخلصة كانت ضمن نطاق مقبول من 0.2 – 0.8 فولت لكل الأجهزة المصنعة، وأعلاها كانت للديود Ag/Si، الخالي من جزيئات النانو. وكذلك كانت قيمة معامل المثالية لكل الأجهزة المصنعة تساوي 1، بينما أظهرت إضافة جزئيات النانو على ديود الشوتكي زيادة في المقاومة على التوالي والمقاومة المجزئة للتيار. على أن قياسات التيار والجهد في حالة وجود الإضاءة على الديود أظهرت تناقصاً في قيمة ارتفاع حاجز شوتكي وانخفاضاً ملحوظاً في المقاومة على التوالي ومقاومة تجزئة التيار.

Table of Contents

Declaration: ... ii
Dedication ... iii
Acknowledgment ... iv
List of Abbreviations and Symbols ... v
Abstract ... vi
List of Figures ... xii
List of Tables ... xiv

1. CHAPTER 1: Introduction ... 1
1.1 Overview ... 1
1.1.2 Doping of Semiconductors ... 3
1.1.3 Charge transport mechanisms in diode junction ... 4
1.1.4 Comparison of Schottky and *p-n* Diodes ... 5
1.2 Significance of the Work ... 5
1.3 Problem Statement ... 6
1.4 Objectives ... 6

2. CHAPTER 2: Previous Studies and Literature Review ... 7
2.1 Diodes and Schottky Diodes ... 7
2.1.1 Diodes ... 7
2.1.2 P-N Junctions: ... 9
2.1.3 Schottky Diode Barrier ... 12
2.1.4 Metal-Semiconductor (MS) contacts and energy bands ... 14
2.1.5 Ohmic Contact: ... 16
2.1.6 Current-Voltage (I-V) Characteristics ... 17
2.1.7 Contact Angle Measurements Between Liquid and Solid Surfaces ... 21
2.2 Theory of Experimental Methodology ... 22
2.2.1 Materials ... 22
2.2.2 Chemical Etching ... 23
2.2.3 Spin Coating for Nanoparticles Deposition ... 25
2.2.4 Metal Deposition ... 26
2.3 Spectroscopic Approach ... 27
2.3.1 Fourier-Transform Infrared (FTIR) Spectroscopy ... 27
2.3.2 Infrared Absorption Process ... 28
2.3.3 Theory of FTIR spectroscopy: Michelson Interferometer ... 29
2.3 Related Previous Studies ... 29

3. **CHAPTER 3: Methodology and Materials** ... 33
3.1 Materials ... 33
3.1.2 Chemicals for etching ... 33
3.1.3 Nanoparticles ... 34
3.1.4 Spin Coating ... 35
3.1.5 Metal Disposition ... 35
3.1.6 Spectroscopic Data Acquisition ... 36
3.1.7 Current-Voltage Instrumentations ... 36
3.2 Diode Building Procedure ... 37
3.2.1 Surface Etching of Silicon ... 37
3.2.3 Metal Evaporation in Vacuum ... 38
3.2.4 Current-Voltage Measurements ... 39

4. **CHAPTER 4: Results and Discussion** ... 41
4.1 Contact Angle Measurements and Surface Modification Test ... 41
4.2 FTIR Analysis ... 43
4.3 Current-Voltage Characterization ... 46
4.3.1 Fitting of the I-V Curves of Ag\NPs\Si Schottky Diodes ... 46
4.3.2 The Effect of Light Illumination on the Schottky Diodes ... 51
4.3.3 Fitting of the I-V Curves of Au\NPs\Si Schottky Diodes ... 56

5. **Chapter 5: Conclusion and Future work** ... 60

References ... 63

A. APPENDIX 1 ... 67

List of Figures

Fig. (1.1): Techniques of nanoparticles production: top-down and bottom-up approaches (Dutka, 2014). ... 2
Fig. (1.2): The color of gold NPs as affected by their size. (Subara & Jaswir, 2018) ... 2
Fig. (1.3): Tunneling and Hopping charge transport in diode junction(Song et al., 2020) ... 4
Fig. (2.1): The current-voltage characteristics of a diode(Boylestad, 2013). ... 8
Fig. (2.2): The diode symbol in circuits (HU, 2010). ... 8
Fig. (2.3): PN junction diode (Boylestad, 2013) ... 9
Fig. (2.4): Effect of applied voltage on a PN junction (a) Forward bias and (b) Reverse bias (Boylestad, 2013). ... 10
Fig. (2.5): Representation of a PN junction diode (Boylestad, 2013) ... 10
Fig. (2.6): a) The p- and n-type regions before junction formation. The electron affinity χ and work functions φ_{sp} and φ_{sn}, along with the Fermi levels. (b) A schematic of the junction and the band profile showing the vacuum level and the semiconductor bands (Mishra & Singh, 2007). ... 11
Fig. (2.7): Schottky Barrier between n-type semiconductor and a metal. The broken line is indicating the Fermi Level (Kittel, 2005b) ... 12
Fig. (2.8): Differences between (a) n-type and (b) p-type semiconductors.(HU, 2010) ... 13
Fig. (2.9): MS contact with applied bias (Pierret, 2006; Sze, 2002) ... 15
Fig. (2.10): Forward Bias. $Is \rightarrow M \gg |IM \rightarrow S| = I0$ (HU, 2010). ... 15
Fig. (2.11): Reverse Bias $Is \rightarrow M \ll |IM \rightarrow S| = I0$ (HU, 2010). ... 16
Fig. (2.12): Schematic IV characteristics of Ohmic Contact (Pierret, 2006; Sze, 2002) ... 16
Fig. (2.13): IV-Characteristics of Schottky diode . (Sze, 2002) ... 18
Fig. (2.14): I-V Characteristics of Schottky contact (in the ideal case) (HU, 2010). ... 18
Fig. (2.15): The model of the circuit with Shunt and series resistances (Tong & Pora, 2016). ... 19
Fig. (2.16): Schematic illustration of simple photovoltaic device (O.K et al., 2018). ... 20
Fig. (2.17): Schematic diagram of the contact angle and interfacial tensions of the three surfaces at the three-phase boundary (Subedi, 2011). ... 21
Fig. (2.18): The crystal structure of ZnO with the lattice parameters a and c indicated (Janotti & Van de Walle, 2009). ... 22
Fig. (2.19): Different results in etching of silicon. (a) Isotropic Etching of silicon; (b) Anisotropic Etching of (100) silicon; (c) Anisotropic Etching of (110) silicon (Wang, 2016). ... 23
Fig. (2.20): anisotropic wet etching of cavities different in shapes and sizes as formed in Si_{111} and Si_{100} wafers (Pal & Singh, 2013). ... 24
Fig. (2.21): Stages of spin coating process (Yilbas et al., 2019) ... 26
Fig. (2.22): Schematic of a typical thermal or electron-beam evaporation system (Martín-Palma & Lakhtakia, 2013). ... 27
Fig. (2.23): Michelson Interferometer (Wang et al., 2012). ... 29
Fig. (3.1): N-type silicon wafer, phosphorus doped used in this study ... 33
Fig. (3.2): Chemicals used for etching, Ethanol, DW and KOH(30%wt) ... 33
Fig. (3.3):Bottle of AuNPs purchased from Sigma Aldrich ... 34
Fig. (3.4): (a) Zinc Oxide nanopowder. (b) Dissolving the ZnO nanopowder in Ethanol. (c) Resulting suspension of ZnO NPs. ... 34
Fig. (3.5): The spin-coater and computer program built in Bethlehem university laboratory by Eng. Nader Adawi ... 35
Fig. (3.6): Thermal evaporator in Bethlehem University. ... 35
Fig. (3.7): (a)Tensor II FTIR Spectrometer from Bruker Optics. (b)Sample in the Spectrometer .. 36
Fig. (3.8): (a) SMU borrowed from Al-Quds University. (b) Set to for I-V Measurements ... 36
Fig. (3.9): (a) the set up of the etching process. (b) keeping the KOH at the temperature of 82°C. 37

Fig. (3.10): (a) the Gold and Metal placed in the crucible. (b) the Si samples fixed at the sample holder. (c) Slowly allowing the current to pass through and cause the heating up of the metal for evaporation (d) the resulted Ag\NPs\Si Schottky diode. (e) the resulted Au\NPs\Si Schottky diode. 38
Fig. (3.11): schematic illustration of the fabricated Schottky diode sample in the circuit. 39
Fig. (3.12): The circuit built to test the I-V characteristics of the fabricated Schottky diodes with 40
Fig. (4.1): Contact angle made on the Si sample before etching = 54.7° 41
Fig. (4.2): Contact angle made on the Si sample before etching = 15.1° 42
Fig. (4.3): Contact angle measurements with etched Si surface (a) AuNPs, (b) ZnONPs........ 42
Fig. (4.4): (a) FTIR spectrum of Au NPs (in citrate buffer). (b) FTIR spectrum of ZnO NPs 43
Fig. (4.5): FTIR spectrum of ZnO NPs (Modified) 44
Fig. (4.6): FTIR spectrum of Au NPs (Modified)........ 45
Fig. (4.7): ModDiode fitting of averaged Ag\Si Schottky Diodes 46
Fig. (4.8): Method of extracting the barrier height for the averaged ModDiode fitting for the Ag\Si. 47
Fig. (4.9): ModDiode fitting of averaged Ag\AuNPs\Si Schottky Diodes 47
Fig. (4.10): ModDiode fitting of averaged Ag\ZnONPs\Si Schottky Diodes........ 48
Fig. (4.11): The IV curves as affected by adding NPs to the Schottky diode........ 49
Fig. (4.12): (a) I-V curves of Ag\Si diode in the dark. (b) **:** I-V curves of illuminated Ag\Si diode51
Fig. (4.13): (a) I-V curves of Ag\AuNPs\Si diode in the dark. (b) **:** I-V curves of illuminated Ag\AuNPs\Si diode 51
Fig. (4.14): (a) I-V curves of Ag\ZnONPs\Si diode in the dark. (b) **:** I-V curves of illuminated Ag\ZnONPs\Si diode 52
Fig. (4.15): ModDiode fitting of averaged Illuminated Ag\Si Schottky Diodes 52
Fig. (4.16): ModDiode fitting of averaged illuminated Ag\AuNPs\Si Schottky Diodes 53
Fig. (4.17): ModDiode fitting of averaged illuminated Ag\ZnONPs\Si Schottky Diodes........ 54
Fig. (4.18): The I-V curves of the light-irradiated diodes with and without NPs. 55
Fig. (4.19): Averaged I-V curves of Au\Si, fitted with ModDiode. 56
Fig. (4.20): Averaged Au\AuNPs\Si Schottky diode with the ModDiode fitting 57
Fig. (4.21): Averaged Au\ZnONPs\Si Schottky diode with the ModDiode fitting 57
Fig. (4.22): Averaged I-V curves of Au\Si Schottky diodes with and without particles 58
Fig. (4.23): Averaged ModDiode fitting of the set with gold and metallised layer, with and without the nanoparticles........ 59

List of Tables

Table (2.1): Three regions of the IR from 0.7μm - 1000μm of wavelength.................................. 28
Table (4.1): Important peaks and functional groups in the ZnO NPs FTIR spectrum 44
Table (4.2): Important peaks and functional groups in the Au NPs FTIR spectrum....................... 45
Table (4.3): Parameters of the averaged Ag\Si data.. 46
Table (4.4): Parameters of the averaged Ag\AuNPs\Si data 48
Table (4.5): Parameters of the averaged Ag\AuNPs\Si data. 48
Table (4.6): Parameters Values as affected by the presence of each nanoparticle with silver as metal:.. 49
Table (4.7) : Parameters of the averaged irradiated Ag\ Si data.. 53
Table (4.8): Parameters of the averaged irradiated Ag\AuNPs\Si data.. 53
Table (4.9): Parameters of the averaged irradiated Ag\ZnONPs\Si data. 54
Table (4.10): Parameters Values as affected by (a) the presence of each nanoparticle and (b) after illumination 55
Table (4.11): Parameters Values in the Au\Si Schottky diode 56
Table (4.12): Parameters Values in the Au\AuNPs\Si Schottky diode... 57
Table (4.13): Parameters Values in the Au\ZnONPs\Si Schottky diode 58
Table (4.14): Parameters Values as affected by the presence of each nanoparticle with gold as metal... 58
Table A.1 Standard deviation Ag\Si Dark 67
Table A.2: Standard deviation Ag\Si Light 67
Table A.3: Standard deviation Ag\AuNPs\Si Dark 67
Table A.4: Standard deviation Ag\AuNPs\Si Light 68
Table A.5: Standard deviation Ag\ZnONPs\Si Dark 68
Table A.6: Standard deviation Ag\ZnONPs\Si Light.. 68

CHAPTER 1: Introduction

The first chapter elaborates about the basic concepts needed to better understand the nature of research, by the introduction of the field of nanotechnology and its applications. Moreover, a thorough description is given for the charge transport mechanisms in a diode junction. Additionally, a brief overview is introduced for comparison between a regular Schottky diode (semiconductor/metal) and pn diodes. Finally, the chapter enlightens the significance of this study, followed by the problem statement and the objective of this thesis.

1.1 Overview

"There is plenty of room at the bottom" was the famous lecture in which Richard Feynman presented the term nanotechnology in 1959 (Feynman, 1992), leading to a number of revolutionary inventions and development in this field. 'Nano' comes from the Greek origin, meaning 'dwarf', but in the scientific terms, 'nano' is known to be a unit prefix in the metric system denoting the factor of 10^{-9}.

In 1994, the following definitions were adopted by the Royal Society/Royal Academy of Engineering Working Group (Society & Engineering, 2004):

> *"Nanoscience is the study of phenomena and manipulation of materials at atomic, molecular and macromolecular scales, where properties differ significantly from those at larger scale."*

Synthesis of nanoparticles is mainly achieved by methods that are divided into two main types, shown in Figure (1.1): the bottom-up approach, which means forming structures using physical and chemical procedures; that is building up atom by atom, forming molecules and clusters.

As for the second approach, it is known as the top-down approach, this method indicates the crushing of large objects, yielding small remains; some of the techniques used in this

approach are lithography, laser-beam processing, and other mechanical techniques (machining, etching, grinding, and milling, etc.) All synthesis techniques depend on the desired chemical features (Dutka, 2014).

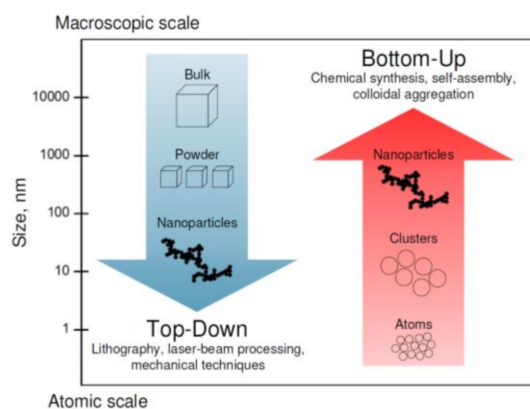

Fig. (1.1): Techniques of nanoparticles production: top-down and bottom-up approaches (Dutka, 2014).

Nanoparticles (NPs) are a vast group of materials having at least one dimension less than 100 nm. Researchers observed the size of the particles influenced the characteristics of the substance, in particular the chemical and the optical properties. Gold (Au) nanoparticles have wine-red color, as shown in Figure (1.2).

The color is dependent on the size of the gold nanoparticles and the thickness of the nanoshell (Khan et al., 2019). This is due the fact that particles with dimensions less than hundred nanometers do not scatter visible light (Whatmore, 2006) at different wavelength depending on the particles size.

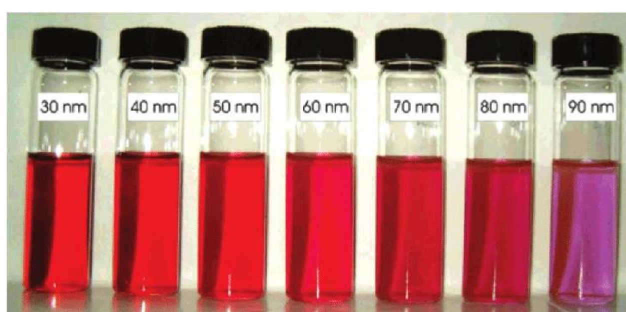

Fig. (1.2): The color of gold NPs as affected by their size. (Subara & Jaswir, 2018)

Describing electrons, in terms of potential wells, energy levels, conduction bands, valence bands, and electron energy band gaps, is known as the *quantum confinement effects*. This

effect is noticed when the particle is too small in size in comparison to the electron's wavelength. The confinement of an electron and hole in nanocrystals greatly depends on the properties of the material (Neikov & Yefimov, 2019).

Semiconductor and metallic nanomaterials have been studied due to their characteristics in linear absorption, nonlinear optical properties, and photoluminescence emission thanks to the quantum confinement effect. Since their properties are different that the equivalent bulk materials, nanoparticles have been the focus of many researches in polymer semiconductor preparations and other possible applications in a number of optoelectronics devices (Kumbhakar et al., 2014).

Nanomaterials are used in the fabrication of electronics. Production is increasing as research is leading to new applications of nanoparticles. More importantly, the use of nanotechnology was beneficial in both human health and environmental aspects.

Some of the applications of nanostructuures in electronics are as following (Allsopp, 2007):

1) Using carbon nanotubes in producing semiconductor chips
2) Examining the different types of nanomaterials in lighting technologies, like light emitting diodes (LEDs)
3) Using 'quantum dots' in laser technology.
4) A number of nanomaterials is used in lithium-ion batteries
5) A possible application in fuel cell and photovoltaics in the solar industry.

1.1.2 Doping of Semiconductors

Semiconductors have a degree of impurities that effect their electrical properties, known as deficit semiconductors. The addition of impurities to the semiconductor is known as doping. In the case of silicon, there are four electrons in the valence band that would form covalent bonds with nearest neighbors. When adding an atom of five electrons in the valence band, e.g. phosphorus, one free valence electron will cause the impurity. Such atoms are known as donors, and the material is n-type. However, the addition of an atom with only three electrons in the valence band, electrons leave behind holes in the semiconductor's valence band, and therefore the material is of p-type (Kittel, 2005).

Adding a few impurity atoms would yield to a compromise in the structure of the crystal, creating a heavily doped structure with strong quantum confinement (Mocatta et al., 2011). Considering low concentrations of doping, roughly below 1015/cm3 in Si, the movement of the carriers does not depend on the doping concentration, and scattering caused by ionized impurities are neglected in comparison with that of the lattice. However, when doping exceeds 1015/cm3 the mobility of the carriers decreases, and the scattering resulting from the impurity, adding extra resistance, cannot be neglected (Pierret, 1996).

1.1.3 Charge transport mechanisms in diode junction

In any diode junctions, charge transport takes place in two mechanisms; tunneling and hopping, shown in Figure (1.3). In the tunneling mechanism, the electrons tunnel consistently through the energy barrier by having enough energy allowing them to pass through. Tunneling I-V for a diode junction can be analysed by using Landauer formula with single electronic state, hence the tunneling transport is linked to the transport properties to the transmission and reflection properties. Furthermore, it is dependent upon temperature and its conductance decreases exponentially with the junction length.

However, as for the hopping mechanism, when the charge is shifted from electrode to nanoparticles, it interacts with the environment of the nanoparticles and its vibrations, gets relaxed and trapped on the junction temporarily, and then hopes to its next position by thermal excitation until reaching the other electrode. In this process, the charge transfers from one electrode to the redox active state and then to the other electrode so that the redox active state switch between reduction and oxidation state continuously. Additionally, it is temperature dependent and its conductance decreases linearly with the length of the junction. (Song et al., 2020)

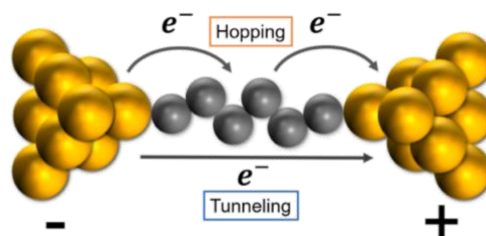

Fig. (1.3): Tunneling and Hopping charge transport in diode junction(Song et al., 2020)

1.1.4 Comparison of Schottky and *p-n* Diodes

Both the $p - n$ diode and the Schottky diode can be used for rectification and non-linear $I - V$ response. The temperature dependence of the Schottky barrier current is quite weak compared to that of a p-n diode. This is because in a *p-n* diode, the currents are controlled by the diffusion current of minority carriers. Also, the Schottky barrier is a majority carrier device that gives it a tremendous advantage over p-n diodes in terms of the device speed, which can reach a few picoseconds in a Schottky barrier. However, the main disadvantage of Schottky diodes is a higher reverse current density. Thus, for a given applied bias, the Schottky barrier is quite large. In addition to the fact that the Schottky barrier quality depends on the surface quality.(Mishra & Singh, 2007)

1.2 Significance of the Work

The embedding of organic nanoparticles in the metal-semiconductor interface is a comparatively more modern way to enhance the performance of the Schottky diode, that is in comparison to traditional ways. Traditional methods may have caused some undesired changes on the interface. These relatively new techniques are preferred due to the simplified steps and the associated cost reasons, moreover due the enrichment these nanoparticles add to the performance of the electronic devices, like photovoltaic cells and perhaps in the future with the bioelectronic devices. (Vilan & Cahen, 2017).

Ohmic and Schottky Si-based electrical interfaces have been studied due to the advantages of silicon over semiconductors of other types. The silicon availability and single crystal of high purity have made it one of the most desired choices for fabricating a number of electronic devices. (Gorji et al., 2015)

Zinc oxide and gold nanoparticles have been gaining attention in the last decade due to their electrical and thermal properties. In this study the influence of embedding ZnO and Au nanoparticles on Ag\Si and Au\Si self-assembled Schottky diodes was studied and an analysis of the important related parameters like ideality factor, barrier height, and series and shunt resistance were carried out.

1.3 Problem Statement

Previously obtained values of the barrier height of Au–Ag alloy–Si contacts varies linearly, from 0.67±0.02 eV to 0.80±0.02 eV. It has been established that the importance of investigating the Schottky diode, and mainly it's barrier height, is due to its link to the work function of the metal, the semiconductor's electron affinity, and the saturation current. (Arizumi et al., 1968).

The embedding of ZnO and Au NPs would reduce the barrier height in the Schottky diode and change the electrical characteristics.

1.4 Objectives

1) Building the Schottky diode using etching, metal evaporation in vaccum.

2) Testing the Current-Voltage characterization of the fabricated Schottky diode.

3) Contact angle characterization as verification of the modification of the semiconductor's surface.

4) Verifying the presence of the nanoparticles on the modified semiconductor's surface prior to metal evaporation in vacuum.

In summary, introducing the most important concepts related to this study, and clarifying the significance and the problem statement of this thesis and its objective, the next chapter explores the detailed theory related to this study, in addition to most recent studies.

CHAPTER 2: Previous Studies and Literature Review

Chapter 2 illustrates the theoretical review of the techniques employed in this study and needed for the adequate analysis of the experimental results in characterizing the assembled Schottky diodes. Firstly, using the etching method of wafer of the silicon by using Potassium hydroxide (KOH). Then, applying the spin coating method to implement the desired layer of nanoparticles on the etched surface of the silicon semiconductor. Additionally, the electrical characteristics of the fabricated diodes, in the absence and presence of the nanoparticles, were determined by using the current-voltage (I-V) measurements. Moreover, the Fourier Transform Infrared (FTIR) Spectroscopy has been utilised to assure the successful deposition in the spin coating process. Thermal evaporation technique has also been used to produce the thin film of the metal on the Schottky diode.

2.1 Diodes and Schottky Diodes

A rectifier, or a *diode*, is an electrical device that works as a converter of alternating current (AC) to direct current (DC) (Kittel, 2005).

2.1.1 Diodes

Diodes are electrical devices consisting of two electrodes, the anode and the cathode, and incline to conduct electric current in one direction only by using P-N junction. Diodes mainly protect the circuits by limiting the voltage, and for non-linear mixing of two voltages such as amplitude modulation, they are considered as voltage rectifiers, and as voltage multipliers, such as double input voltage. Figure (2.1) displays the Current-Voltage characteristics of a diode (Kittel, 2005).

When the anode voltage is greater than the cathode voltage, the diode is forward biased; conducting the current strongly, while the voltage drop across it is independent of the current of the diode, and the effective resistance is small. Otherwise, if the anode voltage is smaller than the cathode voltage, the diode is reverse biased. Hence, it conducts current dimly, the current of the diode is nearly independent of voltage until the breakdown, and the effective

resistance is very large. (Boylestad, 2013) The symbol of the diode in circuits is shown in Figure (2.2).

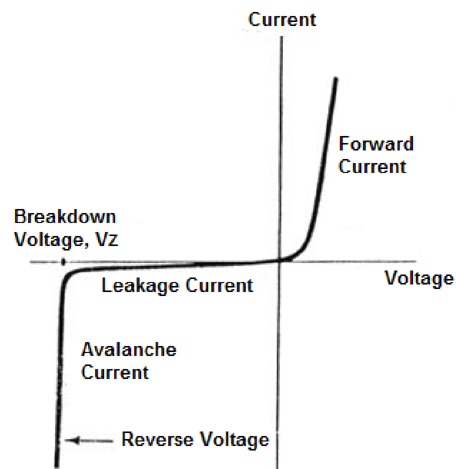

Fig. (2.1): The current-voltage characteristics of a diode(Boylestad, 2013).

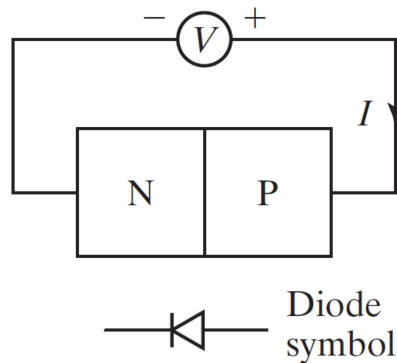

Fig. (2.2): The diode symbol in circuits (HU, 2010).

Thus, there are many semiconductor diodes: Avalanche diodes, constant current diodes, crystal diodes, tunnel diodes, Gunn diodes, light emitting diodes, laser diodes, thermal diodes, pin diodes, photo diodes, junction diodes, and many more.

However, in most cases the basic format for the diode is much the same. The diode contains a PN junction, which provides the basic functionality for the device (Mishra & Singh, 2007).

2.1.2 P-N Junctions:

The p-n junction is one of the most important junctions in solid-state electronics. The junction is used as a device in applications such as rectifiers, waveform shapers, variable capacitors, lasers, detectors, etc.

The following notions are important to better understand how a p-n junction operates (Mishra & Singh, 2007):

i) The carrier distributions for electrons and holes that are in the material.
ii) The physical processes that are responsible for current flow in the structure.

PN-Junctions are formed from a semiconductor piece with one end P type and the other end N type as shown in Figure (2.3). Both ends have different characteristics. One end has an excess of electrons while the other has an excess of holes (Sze, 2002).

When the two regions meet, the electrons in the N-type end will fill the holes in the P-type end and there are no free holes or electrons at the interface. Thus there will be a thin area depleted of charge, called a *depletion region* (Mishra & Singh, 2007) (Kittel, 2005).

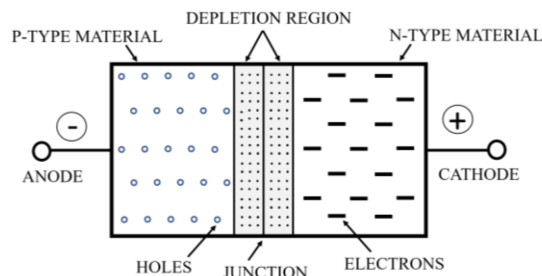

Fig. (2.3): PN junction diode (Boylestad, 2013).

However, the current cannot always flow in the direction that the voltage is applied to the junction. As shown in Figure (2.4), when the voltage is applied such that the P type area becomes positive and the N type becomes negative, holes are attracted towards the negative voltage and electrons move towards the positive voltage and thus jump over the depletion layer; causing the depletion region to decrease. Even though the holes and electrons are moving in opposite directions, they carry opposite charges; representing the same direction of the current (Kittel, 2005).

Nevertheless, when the voltage is applied in the opposite sense no current flows; since the holes and electrons are attracted from the junction itself leading to an increase in the depletion region (Kittel, 2005), as explained in Figure (2.4) b.

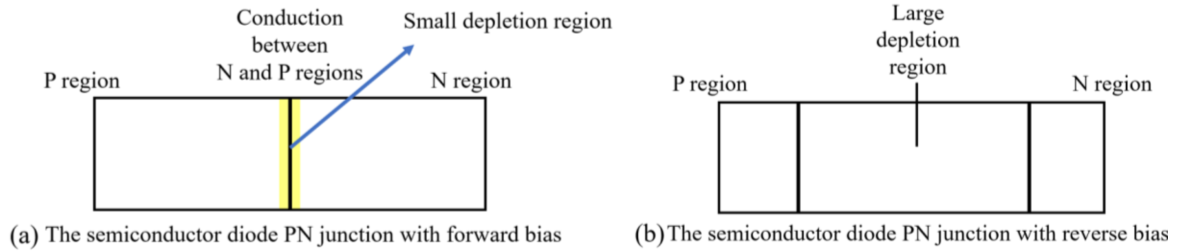

Fig. (2.4): Effect of applied voltage on a PN junction (a) Forward bias and (b) Reverse bias (Boylestad, 2013).

The PN-junction forms a semiconductor device called *PN junction diode,* shown in Figure (2.5), with P region acting as the anode, and the N region as the cathode. Hence, acquiring both types of biases can be obtained by applying an external voltage, making two types of biases, forward biased and reverse biased.

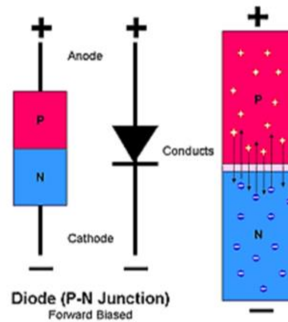

Fig. (2.5): Representation of a PN junction diode (Boylestad, 2013).

The difference of energies between the vacuum levels is called *the work function*, and is denoted by ϕ. The work function indicates the least energy required to extract an electron from the solid or semiconductor.

Moreover, the difference of energies between the vacuum level and the semiconductor's edge of the conduction band is called *the electron affinity*, and is denoted by χ. (Petty, 2007; Sze, 2002) The *barrier height* Φ_B is defined as the energy difference between the band edge with majority carriers and the Fermi energy of the metal (Kittel, 2005; Petty, 2007).

In the metal, there are some electrons, present at the Fermi level E_{F_M}, which is the highest energy level filled in the case of ground state, but this is not the case in the semiconductor, E_{F_s}. Hence, $\Phi_{Metal} > \Phi_{Semiconductor}$ (Kittel, 2005; Petty, 2007; Sze, 2002).

In the case where zero voltage is applied across a junction, called *unbiased junctions*, as shown in Figure (2.6). Every photon that is being absorbed forms an electron and a hole, these carriers, diffusing in the junction, get separated at the energy barrier by the built-in electric field, this separation causes a forward voltage through the barrier (Kittel, 2005). However, at any interface of two different materials. a built-in potential is formed. Nevertheless, the potential net sum of all closed loops would be zero (HU, 2010).

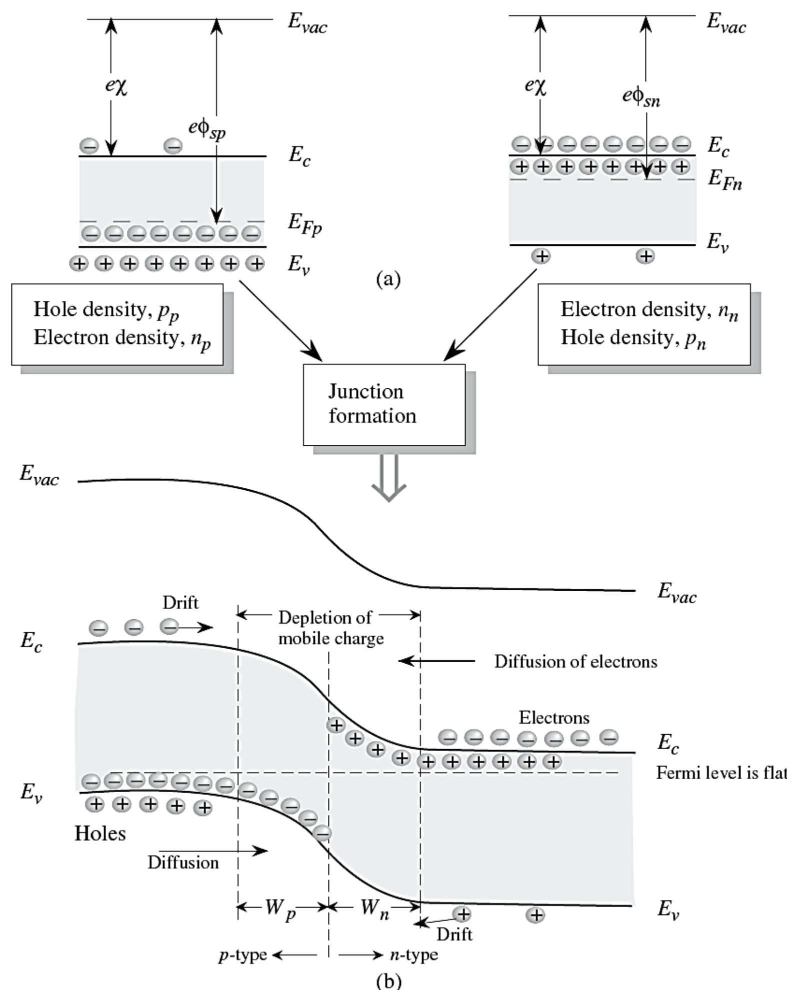

Fig. (2.6): a) The p- and n-type regions before junction formation. The electron affinity χ and work functions φ_{sp} and φ_{sn}, along with the Fermi levels. (b) A schematic of the junction and the band profile showing the vacuum level and the semiconductor bands (Mishra & Singh, 2007).

2.1.3 Schottky Diode Barrier

In the year 1938, W. Schottky noticed a rectifying behavior that was caused from bringing a semiconductor into contact with a metal (Sze, 2002). This potential barrier, now called the *Schottky barrier*, is produced by the accumulation of the transferred electrons at the surface of the metal and leaving behind an electron-depleted region of width W, in which there are uncompensated positively-charged donor atoms creating the previously mentioned depletion area (Petty, 2007; Sze, 2002).

To create Schottky barrier, a metal is thermally evaporated in vacuum onto the semiconductor's surface (Petty, 2007). In Figure (2.7), a case of an *n*-type semiconductor in contact with a metal is illustrated. When bringing these two materials into contact in order to reach thermal equilibrium, two requirements must be fulfilled: The Fermi levels must be equal in both materials, and the continuity of the vacuum level (Sze, 2002).

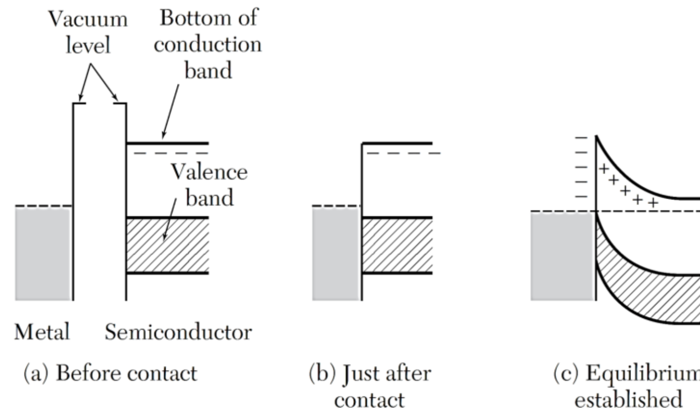

Fig. (2.7): Schottky Barrier between n-type semiconductor and a metal. The broken line is indicating the Fermi Level (Kittel, 2005).

In order to reach this state of thermal equilibrium, electrons in the semiconductor's conduction band become more energetic and can move to the lower energy levels of the metal. This movement causes the accumulation of electrons at the surface of the metal, while at the semiconductor's side; there remain donor ions that are positively charged, and therefore, the region is completely stripped of electrons. When this happens, it causes some bending in the semiconductor's energy bands and therefore lowering the band edges, which is the case in Figure (2.7) (c) (Kittel, 2005; Petty, 2007).

Figure (2.8) shows the difference between the N-type and P-type junctions in the metal/semiconductor contact (Ghabboun, 2004), where E_c is the conduction band, while $E_V$is the valence band (HU, 2010).

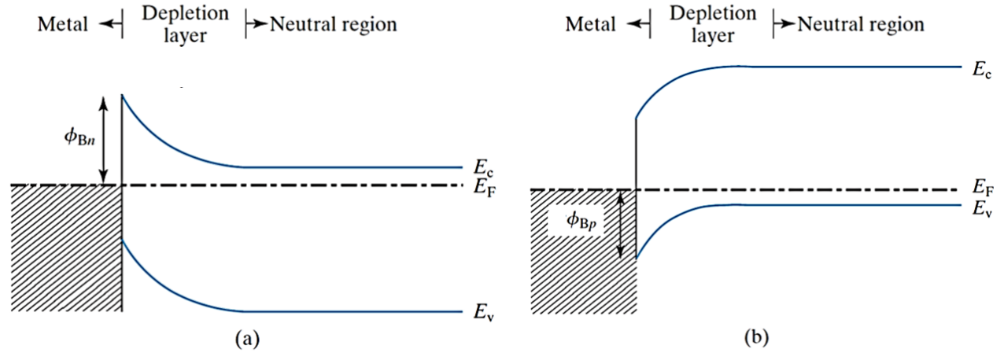

Fig. (2.8): Differences between (a) n-type and (b) p-type semiconductors.(HU, 2010)

Using **Poisson's Equations** to find the distribution of the electric potential given the charge density (HU, 2010), the solution of the equations would be (SI Units), (Kittel, 2005) :

$$\text{div}\, \boldsymbol{D} = \frac{ne}{\epsilon_0} \qquad Eq. (2.1)$$

Where the concentration of the donor is denoted by n. Therefore, determining the electrostatic potential is given by: (Kittel, 2005)

$$\frac{d^2\Phi}{dx^2} = \frac{ne}{\epsilon\epsilon_0} \qquad Eq. (2.2)$$

In consequence, the solution of $Eq. (2.2)$ would be: (Kittel, 2005)

$$\Phi = -\left(\frac{ne}{2\epsilon\epsilon_0}\right)x^2 \qquad Eq. (2.3)$$

If we take the x's origin to the right side of the barrier, for simplicity, the interaction would be at $x = x_b$, as well as relative consideration of the potential energy to the right side would be $-e\phi_0$, yielding the barrier width or thickness as: (Kittel, 2005)

$$x_b = \sqrt{\frac{2\epsilon\epsilon_0|\phi_0|}{ne}} \qquad Eq. (2.4)$$

Now, plugging in the values of each constant, where $\epsilon = 16, e\phi_0 = 0.5$ eV$, n = 10^{16}cm^{-3}$, this would give us the width to be equal to $0.3\mu m$ for Ge as an example (Kittel, 2005).

2.1.4 Metal-Semiconductor (MS) contacts and energy bands

This section considers the MS contacts and energy bands at two cases; at equilibrium and under bias voltage. For the ideal MS contact, we have the following assumptions (Pierret, 2006; Sze, 2002):

1. The metal and the semiconductor are contacted intimately with no oxide or charge layers at the contact point on the atomic scale.
2. No intermixing and inter diffusion between the metal and the semiconductor.
3. No impurities at the MS interface.

i) Zero-Bias:

Under Equilibrium Condition (applied bias V=0), given the fact that $\Phi_M > \Phi_S$, electrons will transfer from the semiconductor to the metal due to their greater energy until the equilibrium condition is established. As in the case of Schottky Barrier, the surface potential-energy barrier (the Schottky barrier height) is a function of the work function of both the metal and the semiconductor at the junction (Pierret, 2006; Sze, 2002):

$$\Phi_B = \Phi_M - \chi \qquad Eq.(2.5) \text{ for N-type semiconductor}$$

$$\Phi_B = \frac{E_g}{q} + \chi - \Phi_M \qquad Eq.(2.6) \text{ for P-type semiconductor}$$

The number of electrons thermally emitted over the potential energy barrier Φ_B from the metal to the semiconductor is equal to the number of electrons thermally emitted over eV_0, with $V_0$is the contact potential from the semiconductor to the metal(Petty, 2007). The barrier results a high resistance when there is even a small-applied voltage.

ii) Bias voltage:

Consider the same case, where $\Phi_M > \Phi_S$ MS contact, a current I will be formed if there is an applied biasing (V_A) on the metal and the connected semiconductor is grounded, as in Figure (2.9).

The current is defined to be positive when it flows from the metal to the semiconductor (Pierret, 2006; Sze, 2002). In this case, we have the following categories; *forward* and *reverse* biasing.

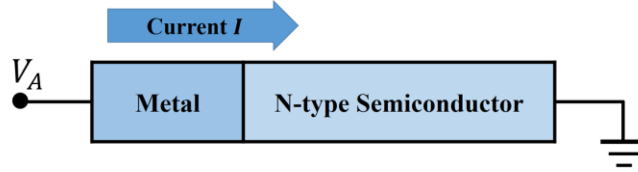

Fig. (2.9): MS contact with applied bias (Pierret, 2006; Sze, 2002)

a) *Forward Biasing* ($V_A > 0$):

When the semiconductor side of the junction is connected to the negative terminal of an external DC power source (like a battery), and the metal to the positive terminal, the effect will be to reduce the contact potential from $V_0 - V$, where V is the the magnitude of the external voltage (Petty, 2007), then it becomes easier for the electrons to overcome the potential energy barrier into the metal.

The resulting current is given by : (HU, 2010)

$$I = I_0 \left[e^{\frac{eV}{k_B T}} - 1 \right] \qquad Eq. (2.7)$$

Where I_0 is a constant related to the barrier height of the metal-semiconductor junction. Therefore, as the V_A is increasing, the current will increase rapidly.(Pierret, 2006; Sze, 2002). In Fig.(2.10), the case where the metal is positive with respect to Si is demonstrated. (HU, 2010)

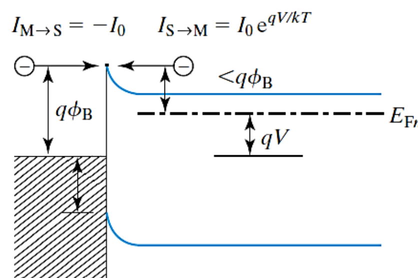

Fig. (2.10): Forward Bias. $I_{s\to M} \gg |I_{M\to S}| = I_0$ (HU, 2010).

b) *Reverse Biasing*$(V_A < 0)$:

In this case, the negative applied bias is on the metal. The Fermi energy of the metal becomes higher than that of the semiconductor, resulting an increasing in the barrier potential across the MS junction, as shown in Figure (2.11). The large barrier will block the diffusion of the electrons from semiconductor to the metal. (Pierret, 2006; Sze, 2002). Under a small reversed bias, only a small amount of electrons in the metal may be able to overcome the potential barrier. (HU, 2010; Pierret, 2006; Sze, 2002). The resulting reverse saturation current is, hence, given by(HU, 2010):

$$I_0 = A^* e^{-\frac{eV_0}{kT}} \qquad Eq.(2.8)$$

A*≈ $100\ A/(\frac{cm^2}{k^2})$ is the Richardson Constant (HU, 2010).

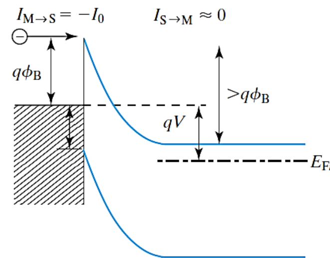

Fig. (2.11): Reverse Bias $I_{S\to M} \ll |I_{M\to S}| = I_0$ (HU, 2010).

2.1.5 Ohmic Contact:

Not all MS contacts can perform as a rectifying Schottky diode, this happens when no potential barrier is formed. The current is capable to flow in both directions of the MS contact, which is known as *The Ohmic contact* (Pierret, 2006; Sze, 2002). Therefore, the Schematic IV characteristics of Ohmic contact is Linear, see Figure (2.12)

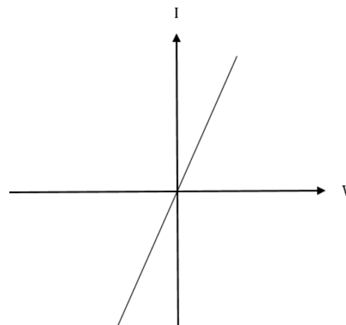

Fig. (2.12): Schematic IV characteristics of Ohmic Contact (Pierret, 2006; Sze, 2002)

An ideal Ohmic contact is a low resistance contact, and non-rectifying junction with no potential barrier existing between the MS interface (Pierret, 2006; Sze, 2002). The contact resistance of a metal/N-Si Ohmic contact is: (HU, 2010)

$$R_c \propto e^{-\left(\frac{4\pi}{h}\emptyset_B\sqrt{\frac{\varepsilon_s m_s}{qN_d}}\right)} \qquad Eq.(2.9)$$

To measure the deviation of practical diodes from ideal thermionic emission model we use a parameter called the *Ideality Factor* and can be expressed as(Gholami et al., 2011):

$$n^* = \frac{q}{KT}\left(\frac{\partial V}{\partial(lnI)}\right) \qquad Eq.(2.10)$$

2.1.6 Current-Voltage (I-V) Characteristics

In order to better comprehend the Schottky diode performance and characteristics, the current-voltage (IV) measurement is a commonly used technique. The importance of providing current-voltage stimulus and measuring the reaction is for showing the threshold voltage and indicating the response of the device to the bias voltage. These devices may be diodes, transistors, sensors, photovoltaic cells, etc. (Kittel, 2005).

Since any real diode does not instantly permit a large current, there can be found some threshold voltage below which there would be a small current, while above that quantity, the current will be large.

Figure (2.13) displays the IV-curve of a Schottky diode, where the vertical line represents the current flow, which is a dependent variable, and the horizontal line signifies the voltage applied across the Schottky diode, considered as an independent variable. The forward current grows exponentially, and the forward voltage drop is between 0.2V and 0.3V (Sze, 2002).

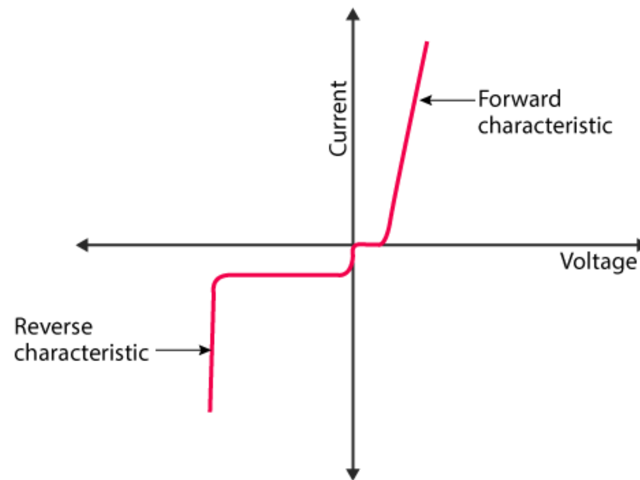

Fig. (2.13): IV-Characteristics of Schottky diode . (Sze, 2002)

In general, the applied voltage defines the flowing current through the Schottky contact. Under a forward bias, when the external voltage exceeds a few $\frac{kT}{q}$ volts, the exponential term will dominate the resulting value of the current.

Whereas for the reverse bias, when the applied voltage is greater than a few $\frac{kT}{q}$ volts, see Figure (2.14) which demonstrates the case of the ideal Schottky diode. The exponential term is neglected, resulting in a small saturated current $I = I_0$ (HU, 2010; Pierret, 2006; Sze, 2002).

The graph shows what happens to the current through a PN junction as the voltage increases. When the voltage is negative, there is a small negative current. When the voltage is positive, the current is also positive and increases rapidly with increasing voltage

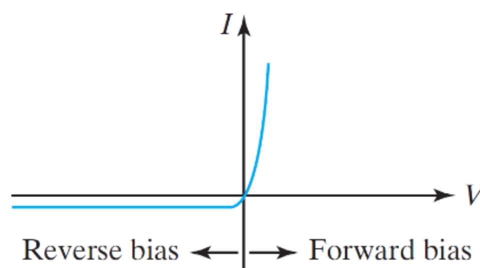

Fig. (2.14): I-V Characteristics of Schottky contact (in the ideal case) (HU, 2010).

In reality, an ideal diode does not exist. therefore, the model shown in Figure (2.15) was modified with the addition of shunt and series resistances. These parameters produce extrinsic effects and hence affect the external behavior of the model. The curve factors in I-V characterisation are lower than ideal, that is mainly due to the series resistance (R_s). As the substrate increases in size, the resistive losses get larger.

However, the curve is not only limited by R_s but also by low shunt resistance (R_{sh}). The shunt resistance is due to leakage across the pn-junction caused by the impurities and crystal defects within the junction region (Tong & Pora, 2016).

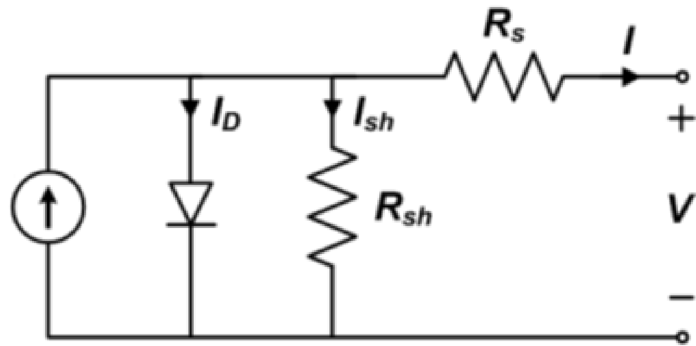

Fig. (2.15): The model of the circuit with Shunt and series resistances (Tong & Pora, 2016).

Therefore, the current in through the Schottky diode in terms of the input voltage and both resistances is given by Eq.(2.11)

$$I = I_s\left[e^{\frac{V-R_sI}{nV_{th}}} - 1\right] + \frac{V - R_sI}{R_{sh}} \qquad Eq.(2.11)$$

Where $V_{th} = \frac{k_BT}{q}$ is called the thermal voltage.

This equation is not solvable in elementary function's analytical methods, therefore, the current's explicit solution and the calculations of the parameters can be found using computer programs (Aazou & Assaid, 2010).

Photovoltaic effect is a course by which the cell alters the absorbed energy of sunlight into electricity, with benefits for a safe environment since it has zero carbon-dioxide emissions. The photon energy absorbed by nanomaterials is transferred to the electrons in the atoms, as shown in Figure (2.16). At a pn-interface, an electric potential is created between n- and p-type semiconductor layers.

When a light photon energy is absorbed by the layer of the semiconductor, as shown in Figure (2.16), it gets transferred to the electrons of the material, giving them sufficient energy to move to the conduction band, leaving a “hole” in the valence band. These valence electrons, after escaping the normal positions in the atoms, join the electric flow or current, and moving towards the negative end, whereas holes move towards the positive direction. When the absorbed available light energy is greater than the bandgap energy of the used material, the atoms collide leading to generating the electrical current due to free moving electrons (O.K et al., 2018).

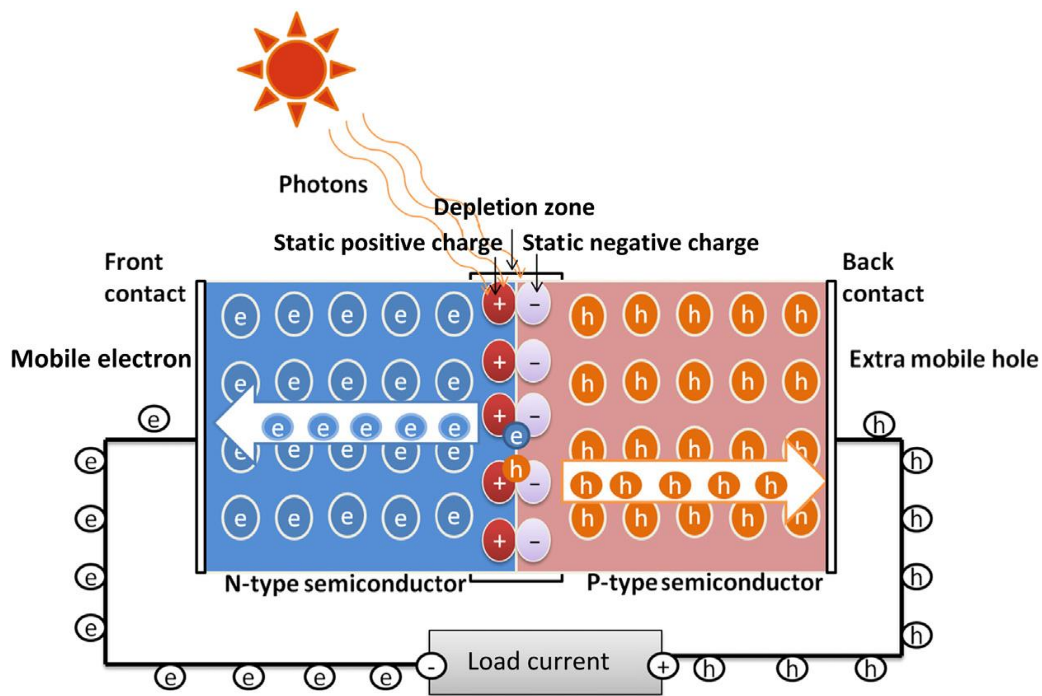

Fig. (2.16): Schematic illustration of simple photovoltaic device (O.K et al., 2018).

2.1.7 Contact Angle Measurements Between Liquid and Solid Surfaces

Contact angle measurement has been used in the study of surface energy, wettability and adhesion of low surface energy materials. The quantitative evaluation of the wetting of a solid by a liquid is made in terms of the contact angle θ. Figure (2.17) shows the schematic diagram for the contact angle and the interfacial tensions at the three phase boundary (Subedi, 2011).

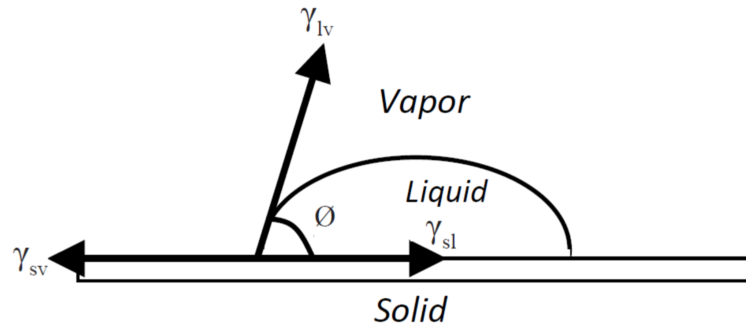

Fig. (2.17): Schematic diagram of the contact angle and interfacial tensions of the three surfaces at the three-phase boundary (Subedi, 2011).

The most important relation regarding the contact angle is the Young's equation that relates the contact angle $\emptyset$, liquid surface tension γ_l, solid surface energy γ_s, solid-liquid surface tension γ_{sl} as expressed in the following equation (Subedi, 2011):

$$\gamma_l \cos \emptyset = \emptyset \gamma_s \gamma_{sl} \qquad Eq.(2.12)$$

A perfect wetting means the maximum value of $cos\theta$ which is achieved when the contact angle is zero. There are two possibilities to inrease the value of $cos\emptyset$, either by reducing the surface tension of the liquid or by increasing the surface energy of the solid.

In the case where the liquid will not wet the solid we say that the surface is hydrophobic and has a poor wettability. If the surface tension of water is lowered by mixing surfactant in it keeping the solid surface unchanged, the contact angle will decrease i.e. water spreads on the surface of the solid (Subedi, 2011).

2.2 Theory of Experimental Methodology

This section of the chapter is concerned about introducing the materials used in this study, in addition to explaining the methodology utilised to execute the successful construction of the Schottky diode

2.2.1 Materials

Zinc oxide (ZnO) nanoparticles, shown in Figure (2.18) is an interesting oxide semiconductor substrate that has been studies widely in the past few years in many applications and researches. ZnO shows unique chemical and physical properties. This metal oxide is environment friendly non-toxic in nature, mostly known for its electrical and optical properties. Moreover, it is preferable because of its optical transparency and its synthesis process as cost effective. Some examples on electronic devices containing ZnO are; thin film transistors (TFTs), sensors photovoltaics, and transparent transistors (Das et al., 2021; Liau & Lin, 2017).

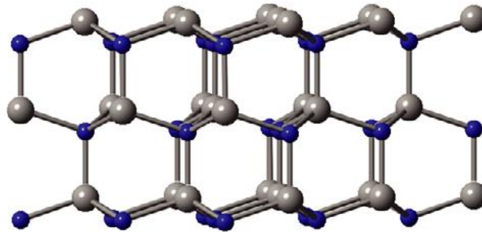

Fig. (2.18): The crystal structure of ZnO with the lattice parameters a and c indicated (Janotti & Van de Walle, 2009).

Recently, there has been an increased interest in examining the use of gold nanoparticles (AuNPs) in new applications, due to the exclusive properties they possess, physically and chemically. The exceptional optical properties are caused by surface plasmon resonance (SPR) effects. This optical phenomenon occurs as a result of electromagnetic wave interacting with the metal's conduction of electrons.

AuNPs are considered as preferable materials in application concerning biomedicine, since they have less toxicity, the fact that they are easily detected, and their compatibility of synthesis, also known as hyperthermia therapy (Herizchi et al., 2016).

Nevertheless, the unusual optical, chemical and electronic characteristics of gold nanoparticles have been attractive for scientists that seek to develop new technologies, particularly in nanoelectronics. Nanoscale gold nanoparticles are used in connecting resistors, conductors, and some other elements of an electronic chip (Sousa et al., 2017) .

2.2.2 Chemical Etching

Etching is the process that is used to remove impurities or selected layers of the semiconductor for the purpose of pattern transfer, wafer polarization, isolation and cleaning (Sze, 1994). There are two fundamental techniques of etching: dry etching (plasma-based etchants) and wet etching (liquid-based etchants) as shown in Figure (2.19)

All unit cells in a single crystal are identical in addition to having fixed orientation. Planes in crystal structures describes their orientation, depending on each unit cell orientation in the crystal. Silicon orientation represents the crystal plane is on the surface on the wafer, it affects the wafer's properties, such as electronic properties. It also denotes the number of atoms on the surface of the wafer, i.e. Si <111> has greater atomic density than that of Si <100> (Angermann et al., 2000). Chemical etching is affected by the orientation of the silicon wafer.

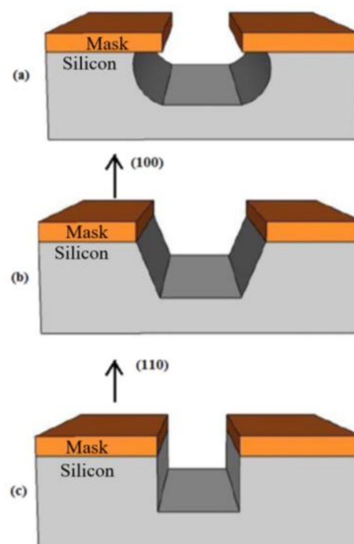

Fig. (2.19): Different results in etching of silicon. (a) Isotropic Etching of silicon; (b) Anisotropic Etching of (100) silicon; (c) Anisotropic Etching of (110) silicon (Wang, 2016).

Dry etching, also called plasma etching, uses reactive ions in a gas phase to dissolve the undesired materials. Thus, it uses plasma instead of liquid etchants (AnoopPrakashA et al., 2013).

Wet chemical etching methods are used when most chemical etchants are liquids. Samples are immersed in the etching solution for a specified time. The etching solutions only removes the film on the exposed areas. The profile of the patterned materials depends on the anisotropy of the chemical etch being used. Wet etchants are in general isotropic, since they etch the film with equal etching rates in all directions. The profiles and etch rates are also controlled by the dispersion of active species to the exposed areas (Sze, 1994). Wet etching provides relatively low costs, which is an important requirement to minimize fabrication cost (Pal & Singh, 2013).

Most etchants consist of an oxidizing agent, like H_2O_2, Br_2, an agent for dissolving the oxides, it may be acid or base like NH4OH, NaOH, HF and H3PO4 (AnoopPrakashA et al., 2013). Alkali metal hydroxides, such as KOH or NaOH, are also considered common etchants for anisotropic of Si etching (Wang, 2016). Potassium hydroxide (KOH) is the perfect anisotropic wet etchant for silicon. In KOH silicon (100) crystal planes are etched 200 times faster than (111) planes. The etching stops when the slow etching of (111) planes meet. The etched depth is dependent on the photoresist mask and the angle, usually 54.7°, between the (111) and (100) planes (Franssila, 2010), illustrated in Figure (2.20)

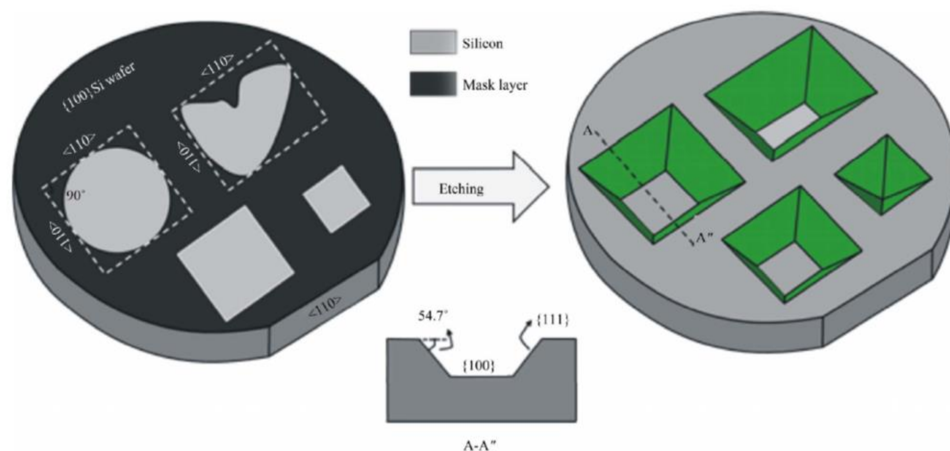

Fig. (2.20): anisotropic wet etching of cavities different in shapes and sizes as formed in Si_{111} and Si_{100} wafers (Pal & Singh, 2013).

The temperature variation and the concentration of the KOH influence the etching results significantly, and may affect the etching rate to be unequal throughout the substrate's surface (Wang, 2016).

2.2.3 Spin Coating for Nanoparticles Deposition

To deposit some nanoparticles on the semiconductor, the spin coater device is widely used today in the microelectronics industry. Spin coating is a method used to form a uniform layer of the on the sample, hence a thin film of the nanoparticle materials will be deposited on the semiconductor.

The spin coating process is divided into four stages, shown in Figure (2.21), as the following:

First, the *deposition*: the required liquid is delivered to be coated to the surface of the substrate. The solution is dropped using microsyringes or micropipettes on a rotating disc holding the substrate. Then, the substrate is accelerated according to the desired speed; spreading the solution due to the centrifugal force, while the height is reduced to a critical height.

The second stage is *spin up*: in this stage, the disc is accelerated to its final desired speed. A twisting motion is produced due to the inertia exerted by the top layer of the fluid while the substrate below is increasing in rotational speed. Eventually, the fluid is thin enough to rotate at the same acceleration and the difference in the thickness is gone.

Then comes the stage of the *stable fluid outflow*: the fluid viscous forces are dominant over the thinning behavior of the fluid, causing the coating to be uniform and outwards. Several parameters are controlling the uniform thickness across the wafer, like the tension of the surface, viscosity of the fluid, the rate of rotation, etc.

The final stage is *evaporation*: this happens due to the loss in the solvent caused by the outflow resulted from the centrifugal force. Hence, with the substrate spinning at a constant rate, the solvent evaporation dominates the coating thinning behavior (Sahu et al., 2009).

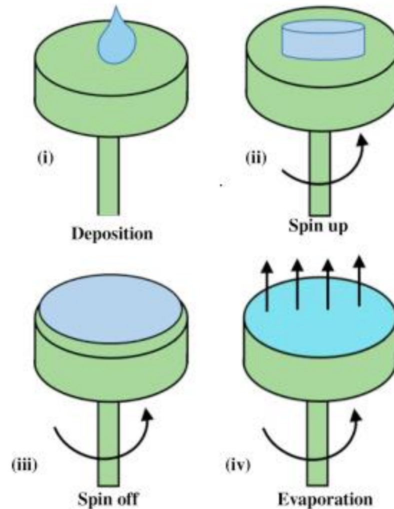

Fig. (2.21): Stages of spin coating process (Yilbas et al., 2019)

2.2.4 Metal Deposition

Thin film can be evaporated from a hot source onto a substrate as shown in Figure (2.22). The evaporation system consists of a vacuum chamber, pump, holding frame for the samples or subsrates, crucible, and a shutter.

A sample of the material that is desired to be deposited on the substrate is placed in the crucible, and vaccum is obtained in the chamber by evacuating it to $10^{-6} – 10^{-7}$ Torr. Then, the crucible is heated by a Tungsten filament or an electron beam to causing the flash-evaporation of the material onto the sample from the crucible. The determination of the film thickness depends on the openning time-length of the shutter.

The evaporation rate of the material is a function of the vapor pressure of the material. Hence, materials that have a low melting point, such as Aluminum, are straightforwardly evaporated, but refractory materials, such as tungsten, need greater temperatures that cause burning of organic films where they land on the sample. With the evaporated material originating from a point source, the resulting films experience shadowing effects, and therefore, producing poor step coverage and nonuniform thickness. In general, evaporated films are highly disordered and have large residual stresses; thus, only thin layers of the materials can be evaporated (Sze, 1994).

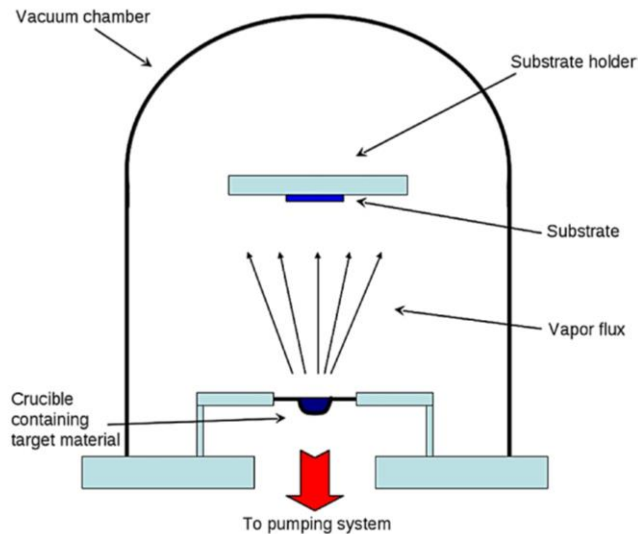

Fig. (2.22): Schematic of a typical thermal or electron-beam evaporation system (Martín-Palma & Lakhtakia, 2013).

2.3 Spectroscopic Approach

Spectroscopy is an experimental field linked to the absorption, emission and scattering of electromagnetic radiations by atoms, nanoparticles and molecules.

2.3.1 Fourier-Transform Infrared (FTIR) Spectroscopy

Fourier transform infrared (FTIR) spectroscopy is a technique used to acquire an infrared spectrum of absorption or emission of a solid, liquid or gas.

The FTIR is beneficial for defining the electronic structure of atoms and molecules (Sathyanarayana, 2004). The term Fourier transform denotes both the representation of the frequency domain followed by the mathematical calculations associated with representing the frequency domain that is initially an interferogram to produce a plot of intensity versus wavenumber, i.e. an infrared spectrum (Griffiths, 2007).

Infrared, in general, is referring to electromagnetic radiation found in the region from 0.7μm - 1000μm of wavelength. The range of the infrared is separated into three regions regarding their location relative to visible spectrum Table (2.1).

Table (2.1): Three regions of the IR from 0.7μm - 1000μm of wavelength

Region	Wavenumber (cm^{-1})	Wavelength (μm)
Near-Infrared	4000-14000	0.7-2.5
Mid-Infrared	400-4000	2.5-30
Far-Infrared	10-100	30-1000

The mid-infrared, that is the region between 2.5μm and 30μm (4000 to 400 cm^{-1}), is the range mostly exploited for chemical analysis in order to study the fundamental vibrations and associated rotational-vibrational structure of the substrate examined (Doyle, 2017).

2.3.2 Infrared Absorption Process

The analysis of the IR spectroscopy helps with determining the chemical functional groups in a sample. When IR radiation passes through the examined sample, absorption taking place causes vibrational transitions between the atoms of molecules that form the sample, this absorption happens when the frequency of applied IR and the natural atomic vibrations frequency are equal.

This leads to changes in the energy on the order from 8 to 40KJ/mole. This amount of energy corresponds to the frequencies of stretching and bending vibration of the bands in most covalent molecules. However, not all the bonds can absorb infrared energy. Only those bonds which have changes of the dipole moment as a function of time (Lorenz-Fonfria, 2020)

The IR absorption spectrum is then graphed as wavelength, or wavenumber, versus transmittance, or absorption intensity. The transmittance (T) equals the ratio of power transmitted by the sample (I) to the power incident on the sample (I_0).

The absorbance (A) is the logarithm to the base 10 of the reciprocal of the transmittance T as shown in Eq.(2.13): (Wilson, 2018)

$$A = log_{10}\left(\frac{1}{T}\right) = -log_{10}(T) = -log_{10}\left(\frac{I}{I_0}\right) \qquad Eq.(2.13)$$

2.3.3 Theory of FTIR spectroscopy: Michelson Interferometer

The optical system in an FTIR spectrometer is very simple: the interferometer requires two mirrors, an infrared light source, an infrared detector, and a beamsplitter. The Michelson Interferometer is the heart of the FTIR device. The key concept of Michelson interferometer is the interaction of waves. If two waves share the same frequency, their peaks and troughs will sum up, forming a constructive interference. In the other hand, if the waves are out of phase, the resulting interference is known to be destructive (Griffiths, 2007) .

This design is based on the original Michelson Interferometer Figure (2.23).

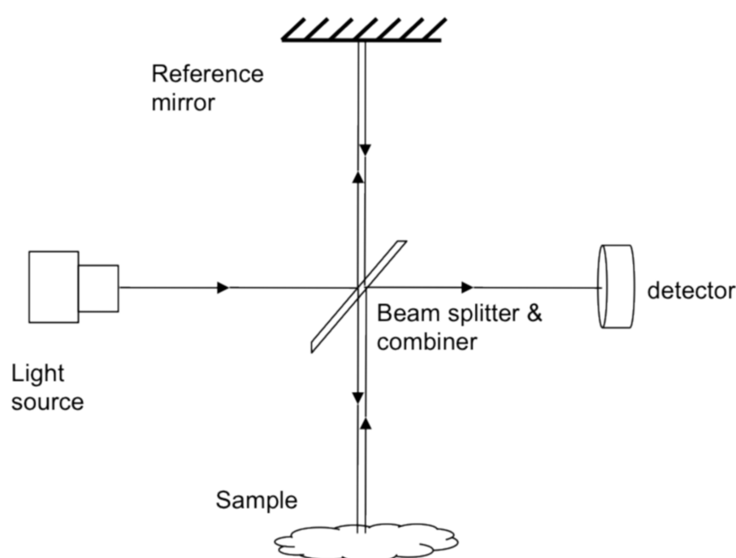

Fig. (2.23): Michelson Interferometer (Wang et al., 2012).

2.3 Related Previous Studies

Labar et al (2022), presented their work in fabrication and electrical analysis of ZnO related to nanostructure-based Schottky device. The fabrication procedure was cost-effective. The properties of the Ni/ZnO junction, studied at 400ºC with silver, forming a metal–semiconductor–metal back-to-back Schottky, Ni/ZnO/Ag; which had rectifying diode behavior for both forward and reverse bias. Electrical parameters were determined based on the back to back Schottky diode model, parameters studied were barrier height, ideality factor, and resistance of a device consisting of two diodes (Labar & Kundu, 2022).

Das et al. (2021) reported two different combining procedures of semiconducting ZnO that modify the patterning of the ZnO materials and their effect on the Schottky diode's photosensing. The study used Al\ZnO\ITO Schottky diodes, investigated the I-V characteristics. The properties of the charge transport were studied through impedance spectroscopy. The results showed improved performance of the device when using ZnO, rod-like, in Schottky diodes, and the detailed analysis of the Al\ZnO junction showed a promising and beneficial use for research in future studies of the metal-semiconductor junctions (Das et al., 2021).

Rouis et al. (2021) reported using metal assisted chemical etching (MACE) in the fabrication of Silicon Nanowires, with various etching time. Their technique aimed to control the patterning of silicon nanowire arrays. They successfully formed Al/SiNWs junction diode, and obtained symmetric (I-V) curves caused by different barrier heights at the two sides of the SiNWs. The study used a metal-semiconductor-metal model to investigate the (I-V) and (C-V) characteristics, the resulting values helped explaining the behavior of electron transport by thermionic field emission method. The existence of interface states, and any other alteration in the surface charge caused by etching were confirmed by voltage dependence of the capacity. The results of the study concluded that the performance of SiNWs is of coherent electrical transport properties when prepared with the MACE method, and may help innovative realization of Si nanostructure-based devices of high performance (Rouis et al., 2021).

Kaufmann et al (2021) introduced a study about Schottky barrier height in addition to the ideality factor in structures containing thin film transistors and Metal/Zinc oxide nanoparticles. Aluminium, gold, and nickel were used as metal layers and the organic-inorganic nanocomposites were used in the fabrication. A numerical computational program was used for the data fitting to extract information about Schottky barrier height and ideality factors for each sample. The nickel metallization appears with the lowest barrier height among the tested metals with some value around 0.3 eV. The utilised method of fitting yielded good fitting accuracy in each metal-semiconductor interface, as the case for gold metallization (Kaufmann et al., 2021).

Abbas et al. (2020) investigated the characteristics of electric transport of a gold (Au)-tip/n-Si based nano Schottky diode, using a (C-AFM), conductive mode atomic force microscope. 10 nm average diameter Au nanoparticles, are monodispersed by spin-coating on the silicon substrate, n-type. The layer of nanoparticles was confirmed by AFM. The I-V asymmetry indicated the improved rectifying behavior of the junction with AuNPs, this is explained by the tunneling current increase at the nanoscale. The study showed in the results the importance of controlling the structure of the interface with nanoparticles to improve the nano-Schottky diode's characteristics (Abbas et al., 2020).

Ramadan, et al. (2020) investigated the accurate determination of the electrical properties of photovoltaic devices by predicting and optimising their performance by studying the alternating current (AC) and direct current (DC) electrical Schottky diode's characteristics of metal-insulator-Si semiconductor type. The basic structure Al/Si TiO2 NiCr were studied, at the aim of using them as photovoltaic devices. The basic diode was then modified by the addition of nano-porous Si and silver nanoparticles as layers, leading to Al/Si+nanoPS/TiO/NiCr and Al/Si+nanoPS+AgNP/TiO2/NiCr structures. The AC electrical properties were studied by the electrochemical impedance spectroscopy and Mott–Schottky analysis, whereas current-voltage measurements determined the DC electrical properties of the diodes. The experimental results yielded a model of an AC equivalent circuit for the three different Metal-Insulator-Semiconductor Schottky barrier diodes, while the most significant electrical parameters were calculated. The results also showed a notable enhancement in the performance of the MIS Schottky barrier diodes when the nanoparticles layers were added, hence their importance in the fabrication of photovoltaic devices (Ramadan & Martín-Palma, 2020).

Boutelala et al. (2020) studied the effect of light on photoelectrical and electrical properties of Al/TiO2/p-Si Schottky diodes. The Al/TiO2/p-Si/Al heterojunction, fabricated by forming a thin film of TiO2 p-type Si wafer, with evaporation of Al as metal, front and back contact. The study used Raman measurement which indicated that bands of TiO2 film are characterized by the anatase phase. The transmittance and optical bandgap of thin film TiO2/bilayer were calculated and found to be 74% and 3.30 eV, respectively. The current-voltage (I–V) measurements of Al/TiO2/p-Si/Al, executed in dark and with a ranged

illumination, from 40 to 100 mW/cm^2, at room temperature. The experiment showed that the structure behaved with a perfect rectifying property in dark. The characteristic parameters of diode were determined, such as ideality factor was found to be 1.91, and barrier height was determined as 0.71 eV. Whereas the calculated series resistance of the device was 17.15 kΩ. Moreover, the effect of light on the photoelectrical properties was studied and the device yielded a photovoltaic behavior. Additionally, the diode had a strong response to the optical illumination so the studied structure could be used in photosensor applications (Boutelala et al., 2020).

This chapter illustrated the theory of the subject, with the most recent studies related to the experiment applied in this study. Chapter three is to elaborate on the detailed methodology and materials used.

CHAPTER 3: Methodology and Materials

This chapter contains two sections. The first describes the materials used in this study, and the apparatus used in the data acquisitions. The second section of this chapter explains the Schottky diode building procedure followed in this study to get the results.

3.1 Materials

Single crystal silicon sheets were used to form the substrate of the diode, shown in Figure (3.1), found in Physics laboratory in Bethlehem University. This n-type silicon is doped with Phosphorus (P). The orientation of the silicon used is <111>, with resistivity of 10-20 Ω cm, and thickness of 450$\pm$10μm.

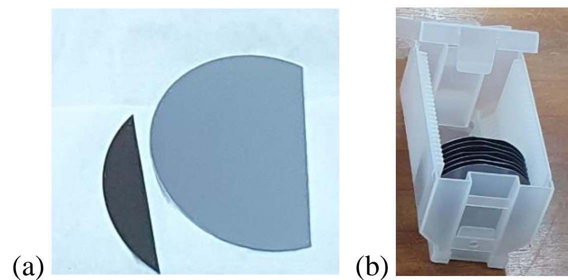

Fig. (3.1): N-type silicon wafer, phosphorus doped used in this study.

3.1.2 Chemicals for etching

Chemicals needed for the silicon substrate etching were distilled water (DW), 95% Ethanol (C_2H_5OH), Potassium hydroxide (KOH) with 30% weight concentration (dissolved in DW). These chemicals were obtained from the Chemistry laboratory at Bethlehem university, see Figure (3.2).

Fig. (3.2): Chemicals used for etching, Ethanol, DW and KOH(30%wt)

3.1.3 Nanoparticles

Gold nanoparticles (AuNPs) were purchased from Sigma Aldrich, in the form of stabilized nanoparticles suspension in citrate buffer, with a concentration of $\sim 6.0 \times 10^{12}$ particles/mL. The size of the nanoparticles is 10nm diameter, maintained at 2-8°C. See Figure (3.3)

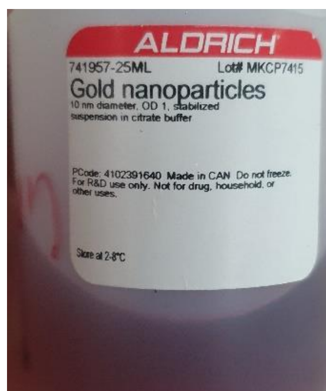

Fig. (3.3):Bottle of AuNPs purchased from Sigma Aldrich.

Zinc Oxide (ZnO) nanopowder was also purchased from Sigma Aldrich, with particle size<100nm as shown in Figure (3.4)a, The nanopowder was then dissolved in 95% Ethanol to obtain a suspension of ZnO nanoparticles with the concentration of 35mM, shown in Figure (3.4)b. The resulting solution, see Figure (3.4)c, is stored at 2-8°C.

Fig. (3.4): (a) Zinc Oxide nanopowder. (b) Dissolving the ZnO nanopowder in Ethanol. (c) Resulting suspension of ZnO NPs.

3.1.4 Spin Coating

Figure (3.5) shows the homemade and calibrated spin coater in the Physics laboratory in Bethlehem University. Each type of the nanoparticles was deposited on the etched silicon substrate with the spin coater by a designed computer program used to control the rounds per minute (rpm) and time.

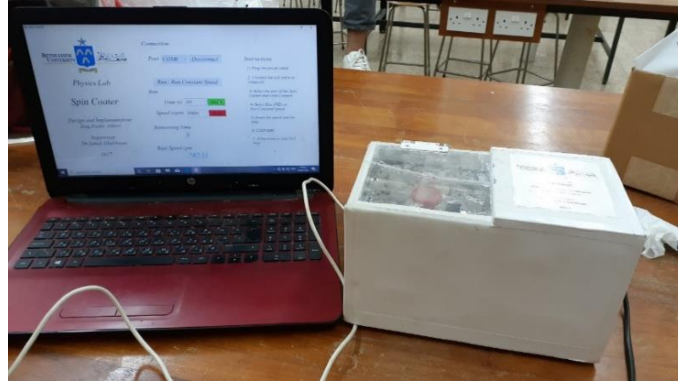

Fig. (3.5): The spin-coater and computer program built in Bethlehem university laboratory by Eng. Nader Adawi

3.1.5 Metal Disposition

In order to place the thin film of metal on the semiconductor/NPs, a thermal evaporation process is needed to be employed in order to complete the device's fabrication. As Figure (3.6) shows, a thermal evaporator was used to complete this step.

Fig. (3.6): Thermal evaporator in Bethlehem University.

3.1.6 Spectroscopic Data Acquisition

As shown in Figure (3.7), TENSOR II FTIR Routine Spectrometer from Bruker Optics at Al-Quds University for the verification of the nanoparticles on the etched silicon samples. The resulting spectra were obtained by Opus 8.1 software and then manipulated using Origin21 software.

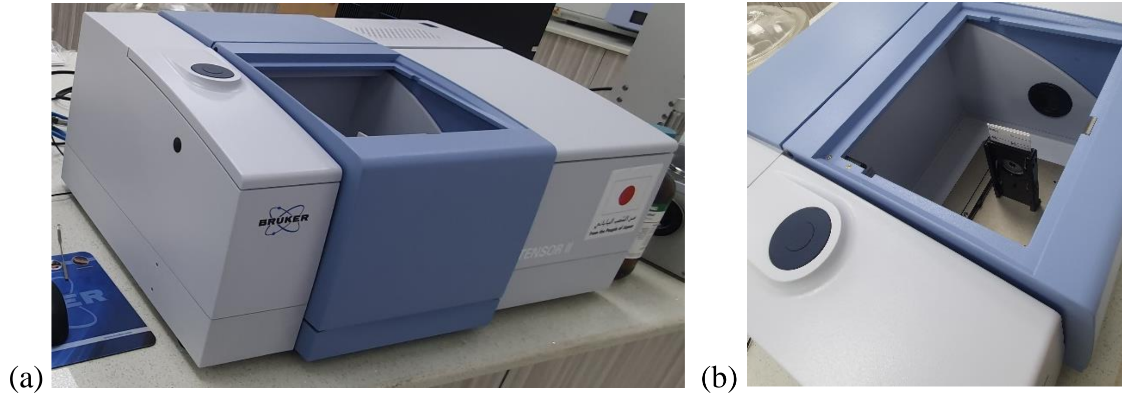

Fig. (3.7): (a)Tensor II FTIR Spectrometer from Bruker Optics. (b)Sample in the Spectrometer

3.1.7 Current-Voltage Instrumentations

Keithley 2400 Standard Series was used as a Source Measure Unit (SMU) Instrument. This SMU instrument, offering measurements of coupled four - quadrant precision voltage and current source, has been borrowed from the Nano lab at Al-Quds University as shown in Figure (3.8)a. The circuit for electrical characterisation was then built using the micromanipulators made at the Physics department at Bethlehem University, as shown in Figure (3.8)b. Silver paint was used to create ohmic contact point with the diode. The resulting graphs were analysed using Origin21 software.

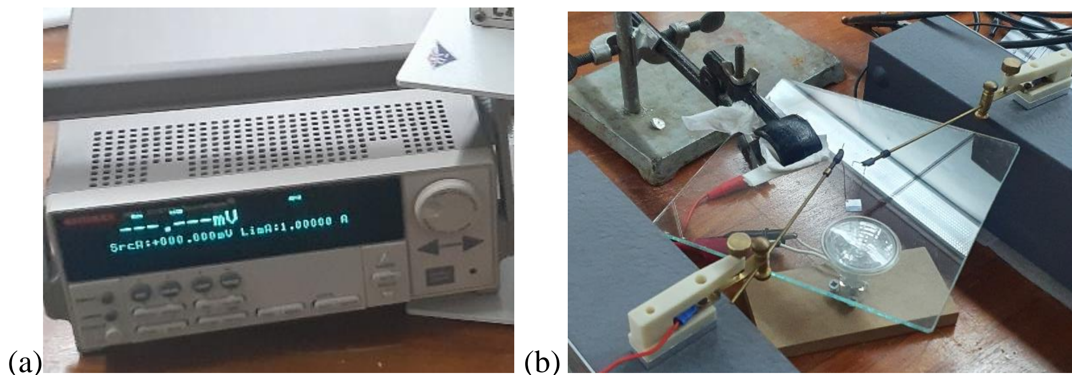

Fig. (3.8): (a) SMU borrowed from Al-Quds University. (b) Set to for I-V Measurements

3.2 Diode Building Procedure

The following section elaborates, in details, the building procedure of the desired Schottky diodes with the nanoparticles.

3.2.1 Surface Etching of Silicon

The substrates of the silicon were made by cutting the silicon wafer into 1.0 cm^2 pieces using the diamond glass cutter pen. The substrates were then immersed in Ethanol (95%) for 30 seconds, followed by immersion in distilled water for another 30 seconds. Then the silicon samples were submerged in KOH (30% wt) solution, of temperature 82°C, heated by a hot plate, for 45 minutes. Then the samples were rinsed in DW, followed by Ethanol (95%) and then left to dry at room temperature. This procedure is illustrated in Figure (3.9).

(a) 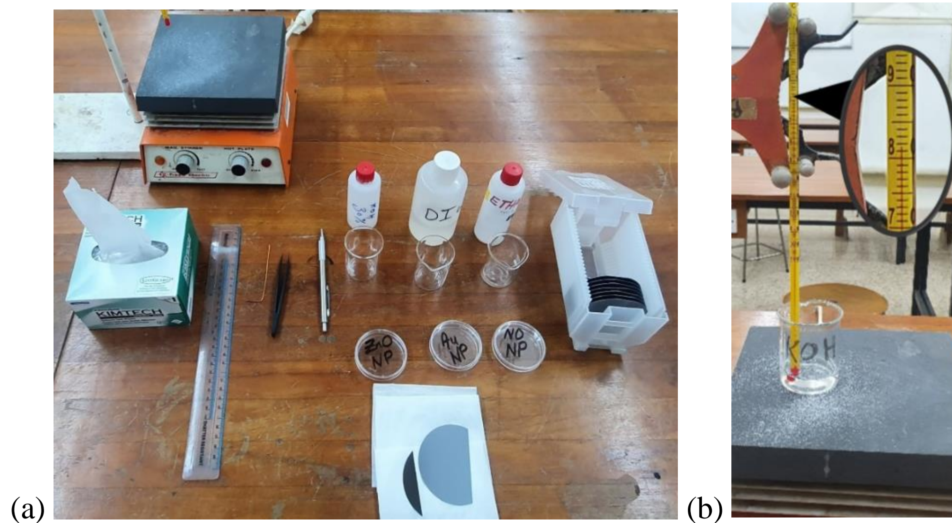 (b)

Fig. (3.9)*:* (a) the set up of the etching process. (b) keeping the KOH at the temperature of 82°C.

3.2.2 Spin-Coating of ZnO and Au Nanoparticles

15 μL of each type of the nanoparticles were dropped on the Si substrate using micropipettes. The Au NPs were spin-coated at the speed of 1200 rpm for 90 seconds, whereas the ZnO NPs were spin-coated for 60 seconds at the speed of 1500 rpm. Before the deposition of the metal thin film, the sample at this point was tested using the FTIR in order to prove the successful coating of the nanoparticles. The deposited film's thickness decreased when the coating speed increased. (Ajadi et al., 2016; Gorji et al., 2015)

3.2.3 Metal Evaporation in Vacuum

Silver and Gold were placed in the crucible, separately, to be evaporated onto the Si substrate. The Bell jar was evacuated to approximately 10^{-6} Torr, the Tungsten filament that is forming the crucible is then heated by slowly allowing the current to pass through the electrodes, causing the metal in the crucible to be evaporated onto the Si substrates that are fixed at the sample holder. This procedure is shown in Figure (3.10)

Fig. (3.10): (a) the Gold and Metal placed in the crucible. (b) the Si samples fixed at the sample holder. (c) Slowly allowing the current to pass through and cause the heating up of the metal for evaporation (d) the resulted Ag\NPs\Si Schottky diode. (e) the resulted Au\NPs\Si Schottky diode.

3.2.4 Current-Voltage Measurements

Both fabricated Ag\NPs\Si and Au\NPs\Si Schottky diodes, and the bare Schottky diodes (without the nanoparticles), were then placed in the circuit setup using the micromanipulators for each back and top contact, resulting in the I-V curves. See Figure (3.11) for the schematic illustration.

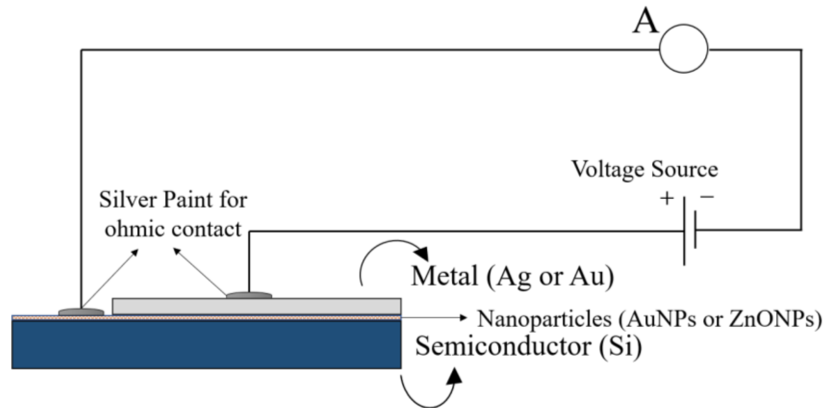

Fig. (3.11): schematic illustration of the fabricated Schottky diode sample in the circuit.

This step was completed using the Keithley SMU and examining the fabricated diodes through the span of -5V to 5V.

Types of samples prepared for this experiment were:

1. Ag/Si
2. Au/Si
3. Ag/ZnO(NP)/Si
4. Ag/Au(NP)/Si
5. Au/ZnO(NP)/Si
6. Au/Au(NP)/Si.

In addition, measurements were taken for the Ag\NPs\Si diodes, to detect the change in the diode's behavior in dark and luminous surroundings, this is to show the effect of light on the behavior of the diodes, these results were then compared to those taken for Schottky diodes with no nanoparticles at the junction. This set up is shown in Figure (3.12)

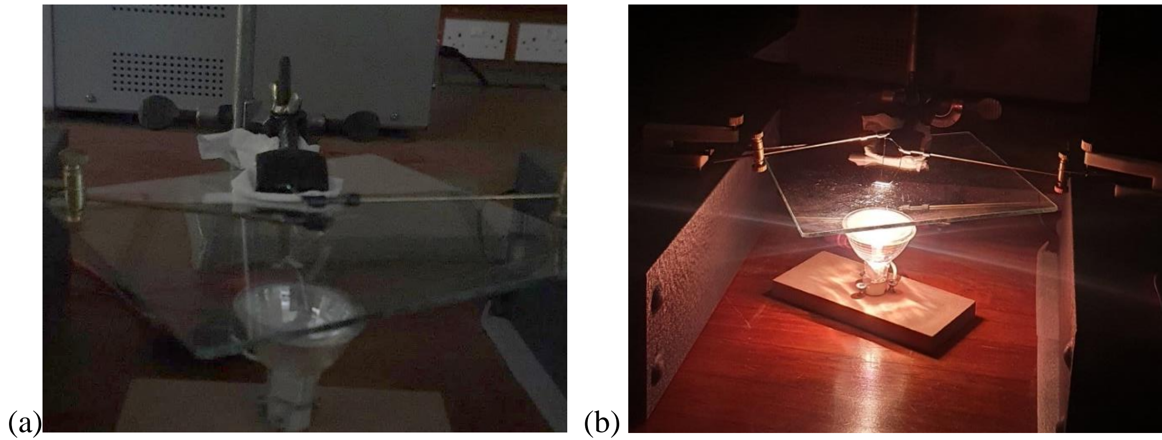

Fig. (3.12): The circuit built to test the I-V characteristics of the fabricated Schottky diodes with and without nanoparticles. (a) in dark surroundings. (b) with added photons.

As chapter 3 has illustrated in details the methodology employed in this study, the next chapter is to extend in results and discussion

CHAPTER 4: Results and Discussion

In this chapter, the experimental results are presented and discussed. The first part is related to the determination of contact angle measurements and modification test to verify the changes of the substrate's surface. The second section will discuss analysis of the obtained FTIR spectra as another technique for NPs deposition. Finally, the third part focuses on the current- voltage curves and their interpretations.

4.1 Contact Angle Measurements and Surface Modification Test

Before etching with KOH, a drop of 30 μL of distilled water was placed on the $Si_{<111>}$ sample, the angle made was 54.7°, as shown in Figure (4.1). Angle measurements were obtained using Physics Tracker software.

Fig. (4.1): Contact angle made on the Si sample before etching = 54.7°

To prove the altering in the Si hydrophobicity after the etching with the KOH, the same volume of distilled water was dropped on the Si sample. The angle is reduced to approximately 15.1° as shown in Figure (4.2).

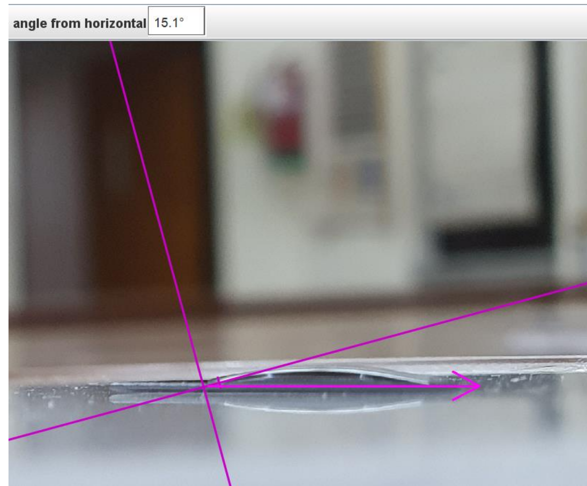

Fig. (4.2): Contact angle made on the Si sample before etching = 15.1°

This indicates that the Si surface became more hydrophilic after etching with KOH for 45 min.

In addition, contact angle measurements were used to test the difference in the surface tension between the ZnO NPs and the Au NPs. Figure (4.3) a, shows the angle made when applying AuNPs, which was equal to 25.7°, while Figure (4.3) b, shows the angle with the Au NPs which was around 14.5°. Since the angle made with the ZnONPs and the Si surface was greater, it is concluded that the surface tension is greater than that of the ZnONPs.

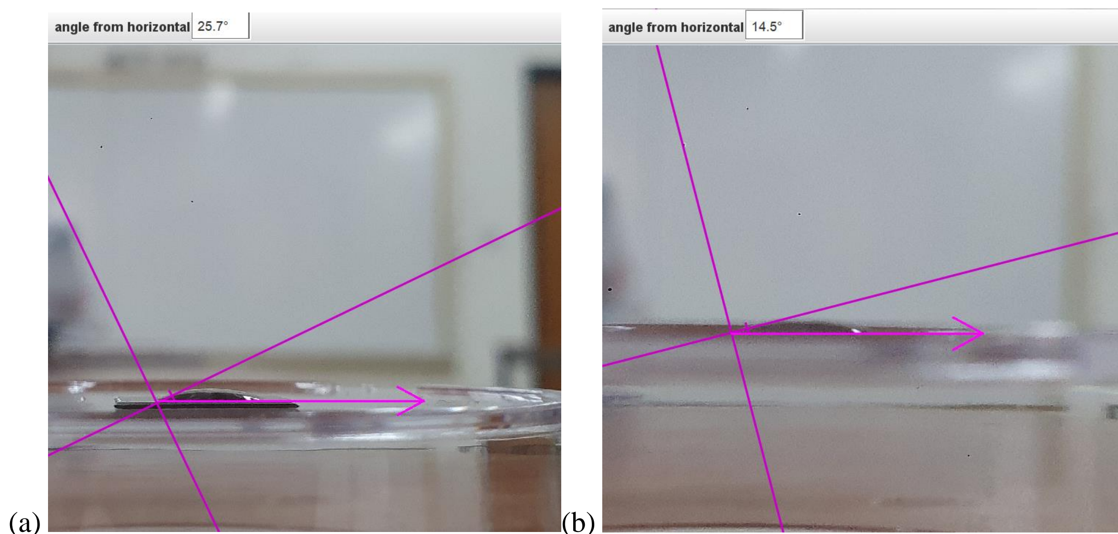

Fig. (4.3): Contact angle measurements with etched Si surface (a) AuNPs, (b) ZnONPs.

4.2 FTIR Analysis

The FTIR spectroscopic approach was used to determine the successful coating of the nanoparticles on the etched Si surface. Figure (4.4) a, shows the Au NPs FTIR Spectrum that resulted from the measurements while Figure (4.4) b, shows the ZnONPs FTIR spectrum.

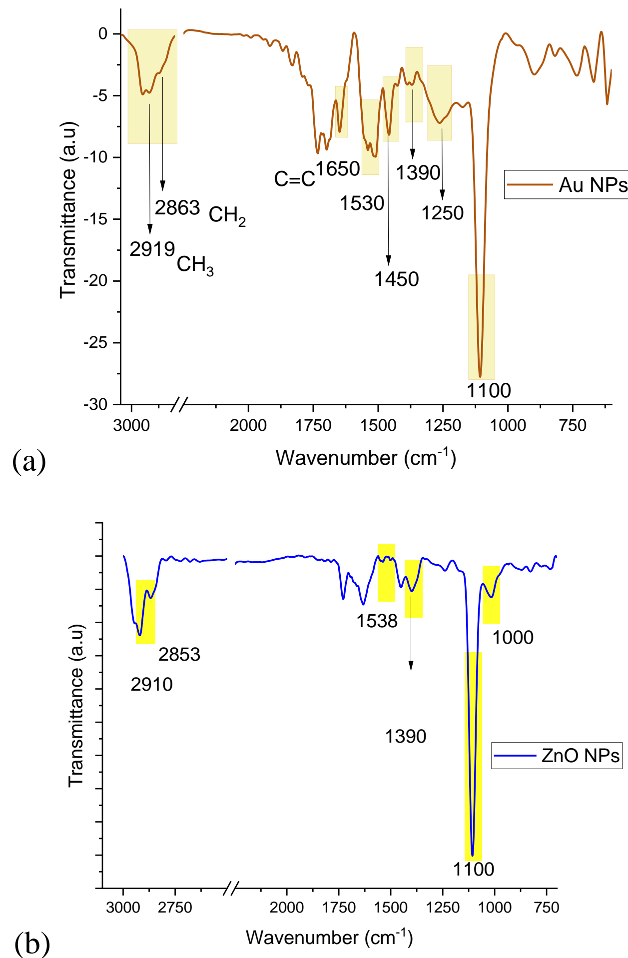

Fig. (4.4): (a) FTIR spectrum of Au NPs (in citrate buffer). (b) FTIR spectrum of ZnO NPs

The different peak intensities and the shifts in the wavenumber in Figure (4.4) are due to the Si contributions at that wavenumber region. The high intensity peak at wavenumber 1100 cm^{-1} denotes the Si-O bonding (Foo et al., 2013), which indicates that the surface of the Si was oxidised in the period of time between the sample preparations and the FTIR measurement. If there is a break in the wavenumber x-axis of the spectrum, it was done to exclude the intense peak of SiO and to see the significant peak ratios to one another, then

the spectra obtained can be analysed. It is obvious that there is an overlap between the results from this study and the spectra extracted from the literature, this overlap is shown in the tables related to each nanoparticle.

As for the ZnO NPs, the FTIR spectrum is as shown in Figure (4.5), followed by Table (4.1) with the important functional groups in the ZnO NPs.

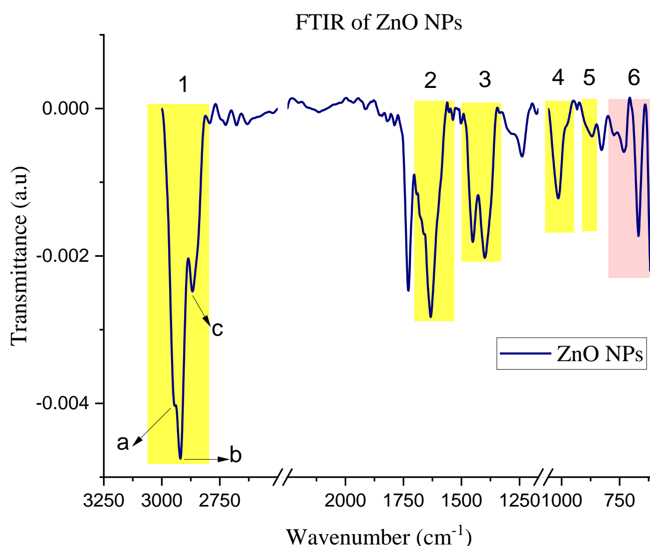

Fig. (4.5): FTIR spectrum of ZnO NPs (Modified)

Table (4.1): Important peaks and functional groups in the ZnO NPs FTIR spectrum

<table>
<tr><th colspan="2">Wavenumber (cm^{-1})</th><th>Functional Group (Vibrations)</th></tr>
<tr><td rowspan="3">1</td><td>(a) 2950</td><td>ν_{as} (asymmetric stretching) CH_3 (Xiong et al., 2006)</td></tr>
<tr><td>(b) 2919</td><td>ν_{as} (asymmetric stretching) CH_2 (Xiong et al., 2006)</td></tr>
<tr><td>(c) 2868</td><td>ν_s (symmetric stretching) CH_3 (Xiong et al., 2006)</td></tr>
<tr><td>2</td><td>1632</td><td>$C = C$ Stretching of an alkane group
(Jayarambabu et al., 2015)</td></tr>
<tr><td rowspan="2">3</td><td>1451</td><td>$C - H$ Bending (asymmetrical) (Hoseinpour et al., 2017)</td></tr>
<tr><td>1384</td><td>$C - H$ Bending (symmetrical)
Zinc carboxylate groups (symmetrical and asymmetrical)
(Xiong et al., 2006)</td></tr>
<tr><td>4</td><td>1012.7</td><td>$C - N$ Stretching (Hoseinpour et al., 2017)</td></tr>
<tr><td>5</td><td>877</td><td>Zn tetrahedral coordination (Jayarambabu et al., 2015)</td></tr>
<tr><td>6</td><td>731-608</td><td>ZnO NPs (Stretching) (Xiong et al., 2006)</td></tr>
</table>

Whereas for the Au NPs, the FTIR spectrum is as shown in Figure (4.6), followed by Table (4.2) with the important functional groups.

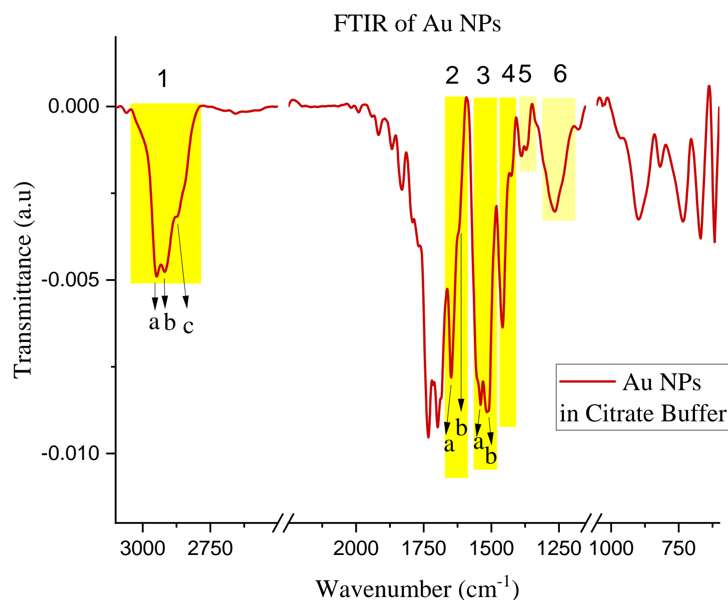

Fig. (4.6): FTIR spectrum of Au NPs (Modified)

Table (4.2): Important peaks and functional groups in the Au NPs FTIR spectrum

Wavenumber (cm^{-1})		Functional Group (Vibrations)
1	(a) 2952	ν_{as} (asymmetric stretching) CH_3 (Mater et al., 2015)
	(b) 2922	ν_{as} (asymmetric stretching) CH_2 (Mater et al., 2015)
	(c) 2852	ν_s (symmetric stretching) CH_3 (Gurunathan et al., 2014)
2	(a) 1649.1	$C = O$ carbonyl group symmetric stretching (Mater et al., 2015)
	(b) 1619.8	$C = O$ carbonyl group asymmetric stretching (Gurunathan et al., 2014)
3	1539	$C - H$ Bending (asymmetrical) (Mohan et al., 2013)
	1511	Aromatic $-C - C -$ groups (Gurunathan et al., 2014)
4	1458	δ(CH2) scissoring (Gurunathan et al., 2014)
5	1392.7	$C - H$ Bending (symmetrical) (Mohan et al., 2013)
6	1265	Ester bond – indicating the Citrate contribution to the spectrum

The resulting spectra indicate that the process of adding nanoparticles is time-sensitive when exposed to air. However, there has been a tolerably successful coating of the nanoparticles of the etched Si surface of the sample.

4.3 Current-Voltage Characterization

OriginPro21 has been used to analyse the I-V curves obtained from the laboratory measurements. Where the average of the readings of each set has been considered and the following calculation and analysis were realized.

Applying ModDiode Fitting to the data, the saturation current I_s, the series resistance R_s, the shunt resistance R_{sh} and the ideality factor n were obtained. Whereas barrier height Φ_b was estimated from I–V data based on the theory of thermionic emission.

4.3.1 Fitting of the I-V Curves of Ag\NPs\Si Schottky Diodes

Figure (4.7) shows the ModDiode fitting of the average of all data obtained from the Ag\Si Schottky diodes obtained for a number of samples and curves, followed by Table(4.3) showing the calculated parameters for the same set.

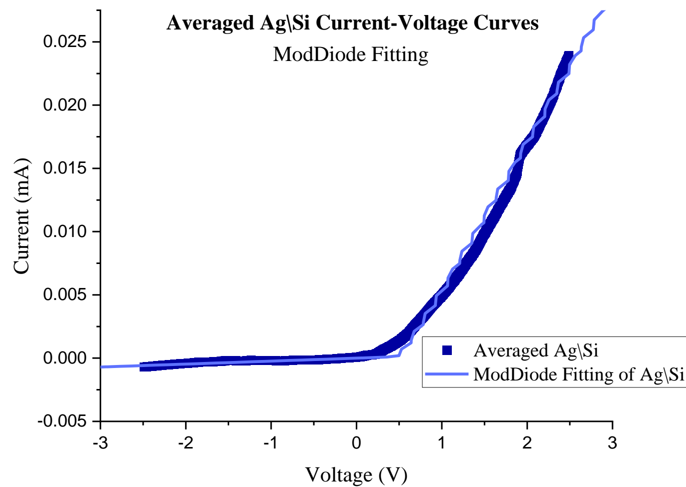

Fig. (4.7): ModDiode fitting of averaged Ag\Si Schottky Diodes

Table (4.3): Parameters of the averaged Ag\Si data.

	Parameter	Value
Voltage, Current Ag\Si	T	300 K
	I_o	4.95633E-13 A
	R_s	82.75792 Ω
	n	1
	R_{sh}	4174.88978 Ω

Also, each reading is fitted with ModDiode, then the averaged fitting is used to extract the barrier height for the Ag\Si Schottky diode, shown in Figure (4.8).

The value of the averaged barrier height is 0.8 eV. This methodology will be used to extract the barrier height value for the rest of the sets.

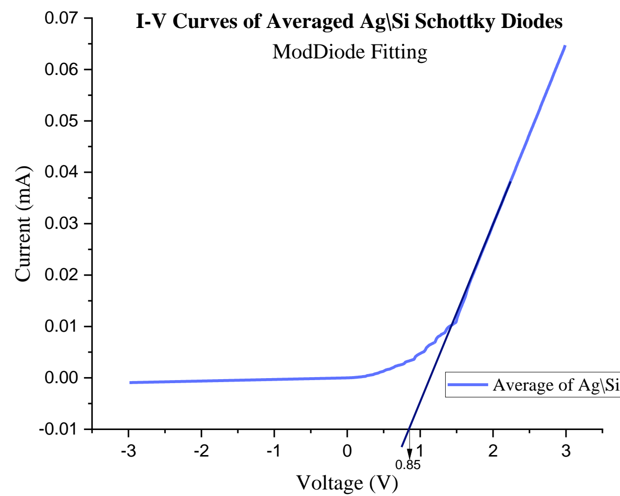

Fig. (4.8): Method of extracting the barrier height for the averaged ModDiode fitting for the Ag\Si.

Repeating the previous method of analysis, Figure (4.9) shows the ModDiode fitting of the average of all data obtained from the Ag\AuNPs\Si Schottky diodes, followed by Table(4.4) showing the extracted parameters for the same set.

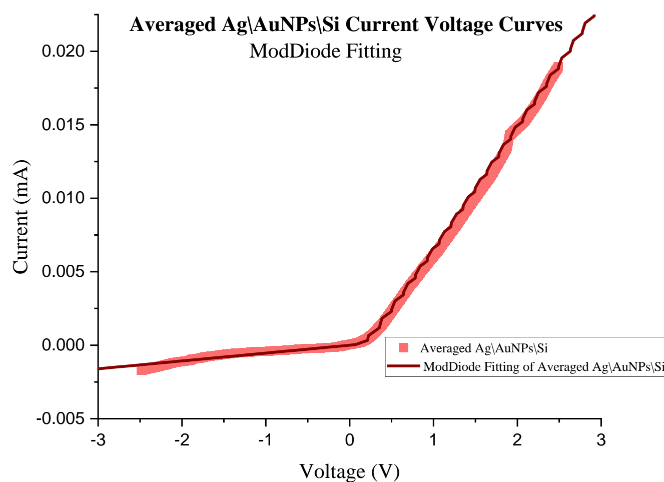

Fig. (4.9): ModDiode fitting of averaged Ag\AuNPs\Si Schottky Diodes

Table (4.4): Parameters of the averaged Ag\AuNPs\Si data

	Parameter	Value
Voltage, Current Ag\AuNPs\Si	T	300 K
	I_o	1.41152E-7 A
	R_s	117.28601 Ω
	n	1
	R_{sh}	1752.47106 Ω

Using the same methodology in Figure (4.8), each reading is fitted with ModDiode, then the averaged fitting curves are used to extract the barrier height for the Ag\AuNPs\Si Schottky diode. The value of the averaged barrier height is 0.29 eV.

Lastly, applying the same steps for the Ag\ZnONPs\Si, Figure (4.10) shows the ModDiode fitting of the average of all data obtained from the measurements of the set, followed by Table(4.5) showing the set's extracted parameters.

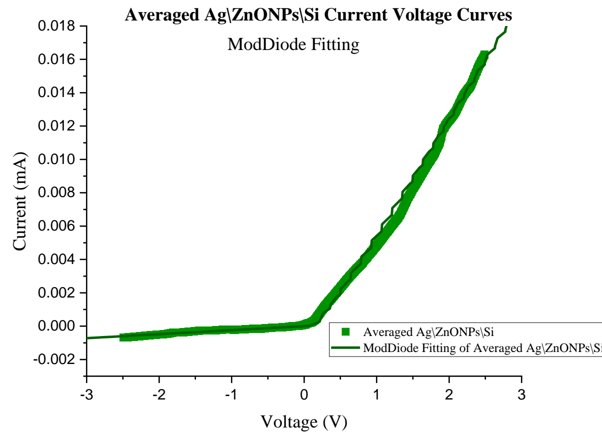

Fig. (4.10): ModDiode fitting of averaged Ag\ZnONPs\Si Schottky Diodes

Table (4.5): Parameters of the averaged Ag\AuNPs\Si data.

	Parameter	Value
Voltage, Current Ag\ZnONPs\Si	T	300 K
	I_o	1.62774E-7 A
	R_s	141.24057 Ω
	n	1
	R_{sh}	4023.08575 Ω

Again, each reading is fitted with ModDiode, then the averaged fitting is used to extract the barrier height for the Ag\ZnONPs\Si Schottky diode. The value of the averaged barrier height for this set is 0.44 eV.

When comparing the parameters as affected by the nanoparticles in the Schottky diode, the results are shown in Table (4.6), and in Figure (4.11):

Table (4.6): Parameters Values as affected by the presence of each nanoparticle with silver as metal:

Parameter	Ag\Si	Ag\AuNPs\Si	Ag\ZnONPs\Si
I_o (A)	4.96E-13	1.41E-07	1.63E-07
R_s (Ω)	82.75792	117.286	141.2406
R_{sh} (Ω)	4174.89	1752.471	4023.086
Φ_b(V)	0.8	0.29	0.44

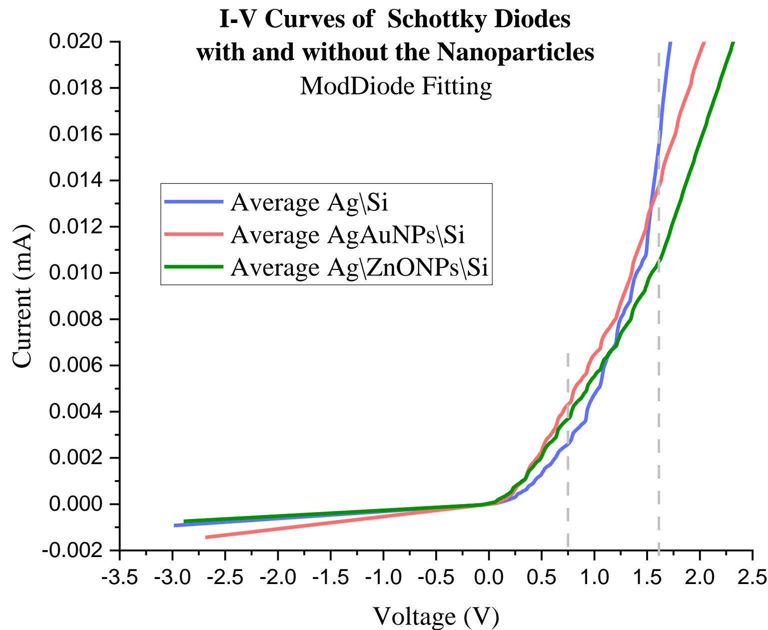

Fig. (4.11): The IV curves as affected by adding NPs to the Schottky diode

Since the saturated current is voltage-independent, and the temperature is constant throughout the experiment, it is noticed that the addition of the nanoparticles to the Schottky diode has contributed in increasing the value of I_o, by facilitating the tunneling of the electrons from metal to semiconductor.

However, the barrier height is decreased in the presence of the nanoparticles as noted in Table (4.6)

The series resistance on the other hand is increased, this means that the charge flow is delayed, and this may affect the quality of the device. This error may be the result of poor etching, and the time-sensitive process between the spin-coating and metal evaporation. This is an indication of a larger length distance between the Schottky barrier and the Ohmic contact. Its origin could be the semiconductor's bulk.

As for the shunt resistance, both nanoparticles contributed in a decrease in its value. However, it is noticed that the decrease in the R_{sh} caused by AuNPs is greater than that caused by the ZnONPs, this means that there is more leakage of the reverse current in circuits with the AuNPs.

Note that the R_{sh} is affected by the metal role at the junction, and since the AuNPs is considered to be metal nanoparticles, this might be the cause of the decrease in the R_{sh} much more than that with the ZnONPs.

As for comparing the forward current values, a cross section is taken at 0.75V, see Figure (4.11), the value of the current in the case of Ag\Si is 0.0026mA, while there is an increase in the current voltage, 0.037mA in the case of Ag\ZnONPs\Si, and 0.0044mA with Ag\ZnONPs\Si. This presents the contribution of the nanoparticles in facilitating the forward movement of electrons from the semiconductor to the metal region.

However, another cross section is taken at 1.6V, the value of the forward current was the lowest with the presence of the NPs, 0.0107mA for Ag\ZnO\Si, and 0.013 for Ag\AuNPs\Si, while the higher value is 0.016mA for the Ag\Si Schottky diode, this is highly affected by the increase of the series resistance and the result of poor etching process.

4.3.2 The Effect of Light Illumination on the Schottky Diodes

I-V measurements were taken for the three types of fabricated Schottky diode, Ag\Si, Ag\AuNPS\Si and Ag\ZnONPs in the presence and absence of illumination, i.e. with a light source aimed at the diode during the measurement procedure. The Schottky diodes were irradiated by a light source of the intensity of $1000\,\frac{W}{m^2}$. The curves below show multiple readings for the same sample in the purpose of comparing the I-V curves with and without illumination.

Figure (4.12) a and Figure (4.12) b illustrate the I-V curves of the Ag\Si Schottky diodes in the dark and the I-V curves of the samples with light irradiation.

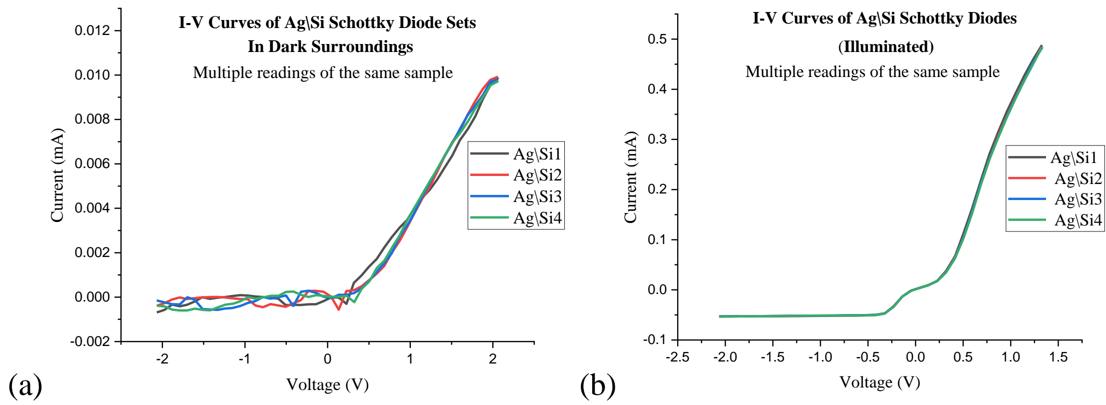

Fig. (4.12): (a) I-V curves of Ag\Si diode in the dark. (b) **:** I-V curves of illuminated Ag\Si diode

Also Figure (4.13)a and Figure (4.13)b demonstrate the I-V curves of the Ag\AuNPS\Si Schottky diodes in the dark and the I-V curves of the same samples but with irradiation.

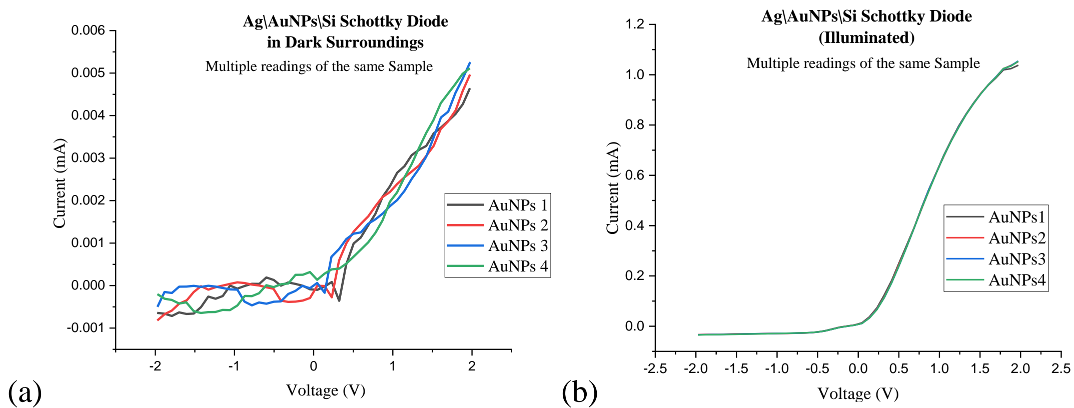

Fig. (4.13): (a) I-V curves of Ag\AuNPs\Si diode in the dark. (b) **:** I-V curves of illuminated Ag\AuNPs\Si diode

Finally, Figure (4.14) a, and Figure (4.14) b exemplify the I-V curves of the Ag\ZnONPs\Si Schottky diodes in the dark and the I-V curves of the same samples but with irradiation.

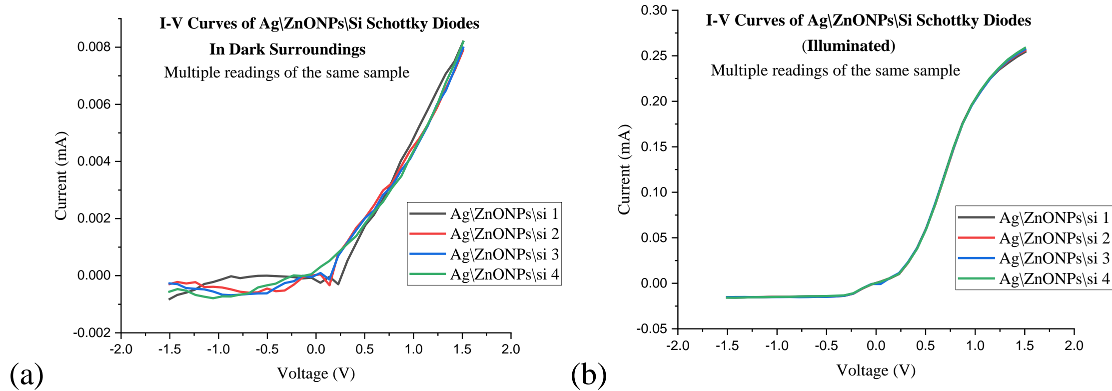

Fig. (4.14): (a) I-V curves of Ag\ZnONPs\Si diode in the dark. (b) **:** I-V curves of illuminated Ag\ZnONPs\Si diode

There are two differences between each pairs of the graphs. The first is that the obvious behavior of the multiple readings of the same sample of the Ag\Si, Ag\AuNPs\Si, Ag\ZnONPs\Si Schottky diodes, to be more in unison when illuminated than that of the same diodes in dark surroundings. The second difference is the increase in the current value, by a factor of 10^3, this can be explained by the fact that the irradiation of the diodes with light has caused a change in the energy gap allowing the electrons in Fermi level to move more easily.

Now, the parameters and the barrier height for each set are obtained by repeating the same methodology in analysis and calculation and extraction previously mentioned by ModDiode fitting. Results related to Ag\Si illuminated Schottky diodes are shown Figure (4.15), and Table(4.7).

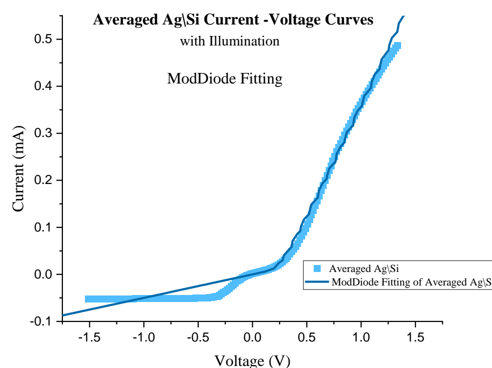

Fig. (4.15): ModDiode fitting of averaged Illuminated Ag\Si Schottky Diodes

Table (4.7) : Parameters of the averaged irradiated Ag\ Si data.

	Parameter	Value
Voltage, Current Ag\Si With light	T	300 K
	I_o	3.38083E-6 A
	R_s	1.99605 Ω
	n	1
	R_{sh}	18.0643 Ω

The barrier height is found to be 0.45eV

Results related to Ag\AuNPs\Si illuminated Schottky diodes are shown Figure (4.16), and Table(4.8).

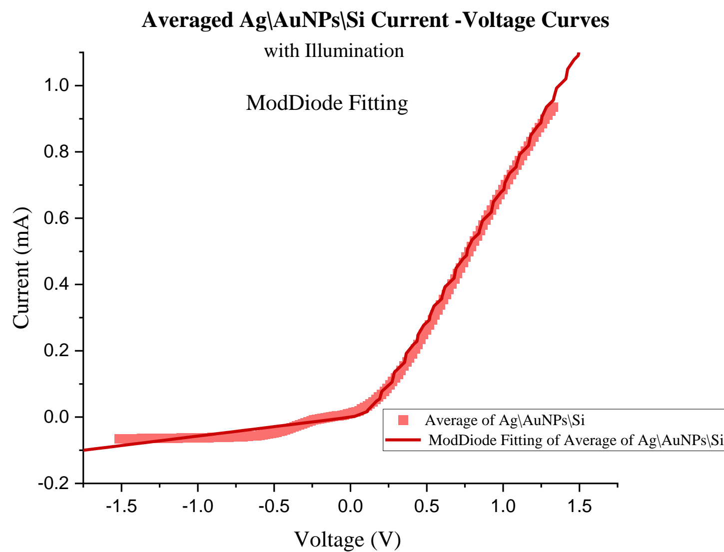

Fig. (4.16): ModDiode fitting of averaged illuminated Ag\AuNPs\Si Schottky Diodes

Table (4.8): Parameters of the averaged irradiated Ag\AuNPs\Si data.

	Parameter	Value
Voltage, Current Ag\AuNPs\Si With light	T	300 K
	I_o	3.09269E-4 A
	R_s	1.17951 Ω
	n	1
	R_{sh}	16.37349 Ω

The barrier height is found to be 0.33eV

Results of the Ag\ZnONPs\Si illuminated Schottky diodes are shown Figure (4.17), and Table(4.9).

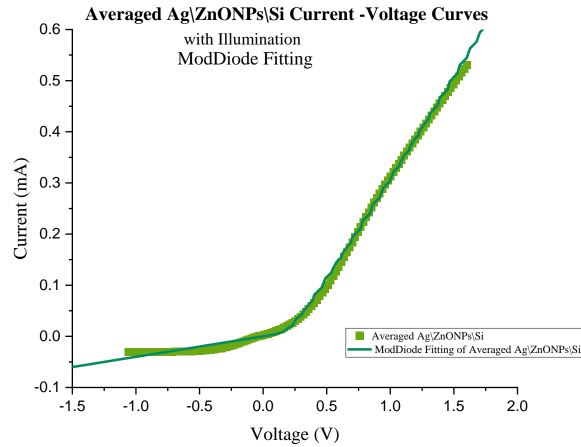

Fig. (4.17): ModDiode fitting of averaged illuminated Ag\ZnONPs\Si Schottky Diodes

Table (4.9): Parameters of the averaged irradiated Ag\ZnONPs\Si data.

	Parameter	Value
Voltage, Current Ag\ZnONPs\Si With light	T	300 K
	I_o	1.05322E-5 A
	R_s	2.43426 Ω
	n	1
	R_{sh}	22.53968 Ω

The barrier height is found to be 0.37eV

The experimental findings show that the prepared diodes are sensitive to illumination and have photovoltaic behavior. Table (4.10) shows the parameters in comparison between the in-dark and after irradiating the diodes. It is noted for the value of the saturation current is much greater with the illuminated samples.

The addition of the nanoparticles also yielded an increase in the value of I_o, however the AuNPs had the greater value. The series and shunt resistance were much smaller in value than that in dark surroundings. The I-V curves of the light-irradiated diodes are shown in Figure (4.18). The graph shows the greater value of the forward current obtained with the AuNPs, whereas the least leakage in reverse bias was obtained with the ZnONPs.

These differences were previously noted with the I-V characteristics with the tested diodes in dark surroundings. Barrier heights results show a decrease for the bare Ag\Si upon illumination, while for the Ag\AuNPs\Si a slight increase is noted, whereas for Ag\ZnONPs\Si the barrier height decreases.

Table (4.10): Parameters Values as affected by (a) the presence of each nanoparticle and (b) after illumination

(a) In Dark	**Ag\Si**	**Ag\AuNPs\Si**	**Ag\ZnONPs\Si**
I_o (A)	4.96E-13	1.41E-07	1.63E-07
R_s (Ω)	82.75792	117.286	141.2406
R_{sh} (Ω)	4174.89	1752.471	4023.086
Φ_b(V)	0.8	0.29	0.44
(b) With illumination	**Ag\Si**	**Ag\AuNPs\Si**	**Ag\ZnONPs\Si**
I_o (A)	3.38083E-6	3.09269E-4	1.05322E-5
R_s (Ω)	1.99605	1.17951	2.43426
R_{sh} (Ω)	18.0643	16.37349	22.53968
Φ_b(V)	0.45	0.33	0.37

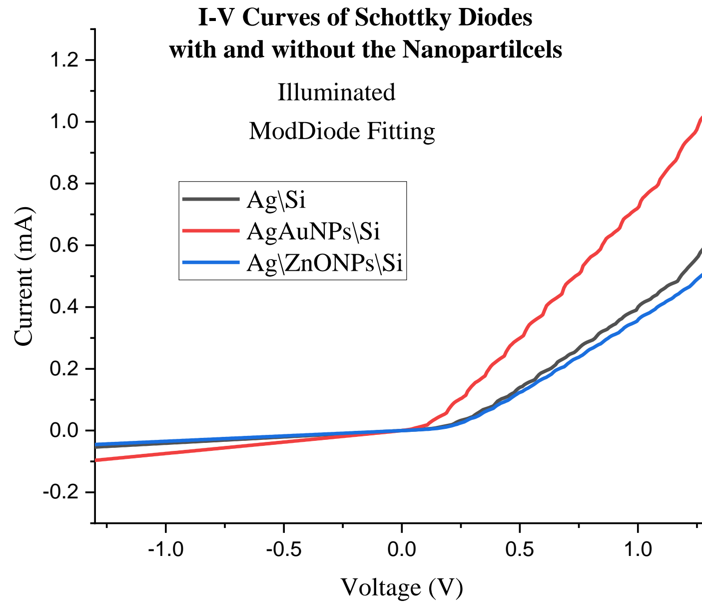

Fig. (4.18): The I-V curves of the light-irradiated diodes with and without NPs.

4.3.3 Fitting of the I-V Curves of Au\NPs\Si Schottky Diodes

The same method of calculations has been used to find the parameters for the Schottky diodes fabricated with the evaporated layer of gold.

The averaged I-V curves of Au\Si Schottky diode, fitted with ModDiode in OriginPro21 as well, is shown in Figure(4.19), while Table(4.11) follows with the resulting parameters.

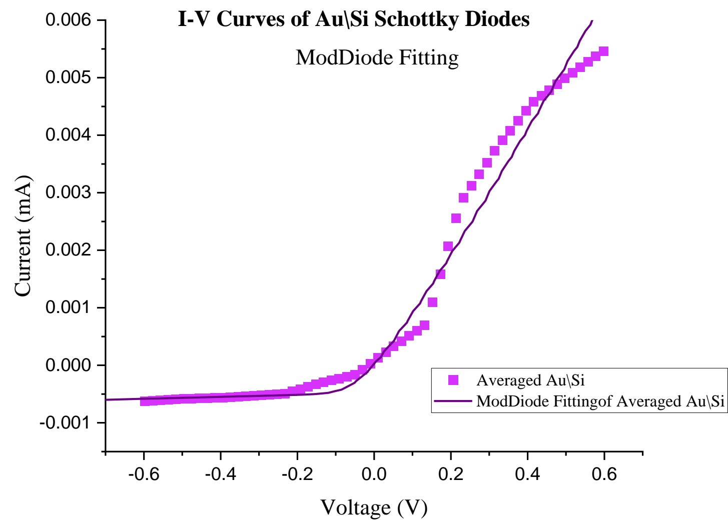

Fig. (4.19): Averaged I-V curves of Au\Si, fitted with ModDiode.

Table (4.11): Parameters Values in the Au\Si Schottky diode

	Parameter	Value
Voltage, Current Au\Si	T	300 K
	I_o	4.87938E-4 A
	R_s	84.16632 Ω
	n	1
	R_{sh}	5850.91793 Ω

Whereas the averaged I-V curves of Au\AuNPs\Si Schottky diode, also fitted with ModDiode in OriginPro21, is shown in Figure (4.20), followed by Table (4.12) with the resulting parameters.

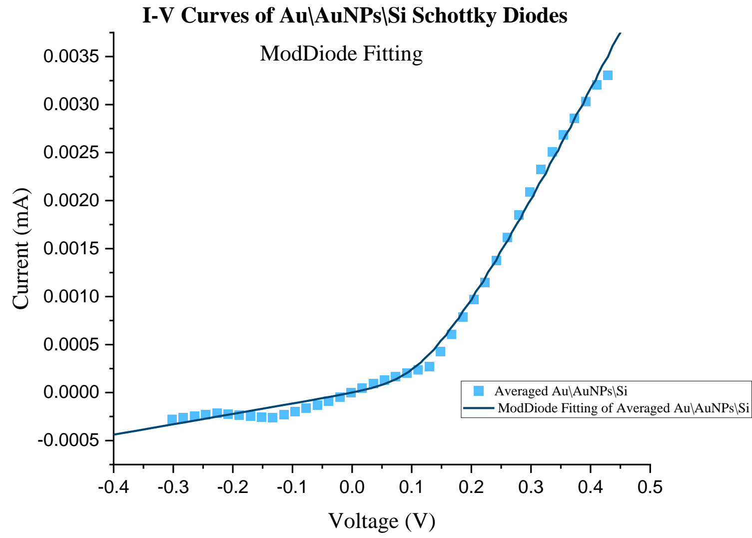

Fig. (4.20): Averaged Au\AuNPs\Si Schottky diode with the ModDiode fitting

Table (4.12): Parameters Values in the Au\AuNPs\Si Schottky diode

	Parameter	Value
Voltage, Current Au\AuNPs\Si	T	300 K
	I_o	6.09186E-6 A
	R_s	76.18738 Ω
	n	1
	R_{sh}	847.08824 Ω

Finally, the averaged I-V curves of Au\ZnONPs\Si Schottky diode is illustrated in Figure (4.21), with the ModDiode fitting. Table (4.13) follows with the resulting parameters.

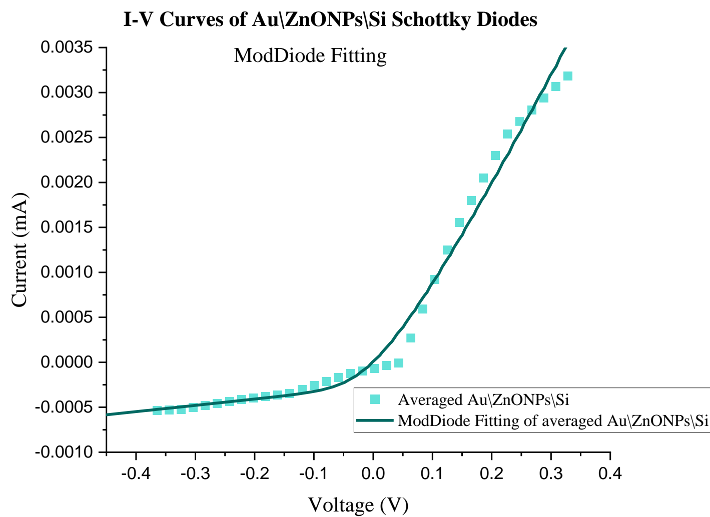

Fig. (4.21): Averaged Au\ZnONPs\Si Schottky diode with the ModDiode fitting

Table (4.13): Parameters Values in the Au\ZnONPs\Si Schottky diode

	Parameter	Value
Voltage, Current Au\ZnONPs\Si	T	300 K
	I_o	2.83982E-4 A
	R_s	74.034
	n	1 Ω
	R_{sh}	1358.28204 Ω

Table (4.14): Parameters Values as affected by the presence of each nanoparticle with gold as metal.

Parameter	**Au\Si**	**Au\AuNPs\Si**	**Au\ZnONPs\Si**
I_o (A)	4.87938E-4	6.09186E-6	2.83982E-4
R_s (Ω)	84.16632	76.18738	74.034
R_{sh} (Ω)	5850.91793	847.08824	1358.28204

After averaging the data obtained in the I-V characterization, it is noted that the presence of nanoparticles has cause a decrease in the values of each parameters. The AuNPs has produced the least value of saturation current; which may be caused by the role intersection between the metal layer of gold and the AuNPs, leading to a possible further seeping of metal at the interface. This may also be the explanation of AuNPs having the lowest value of the shunt resistance as well.

Figure (4.22) illustrates the averaged data obtained from the I-V curves from the gold metallised layer of the Schottky diode, with and without the nanoparticles, followed by Figure (4.23) that compares the averaged ModDiode fitting of the Schottky diodes in the set.

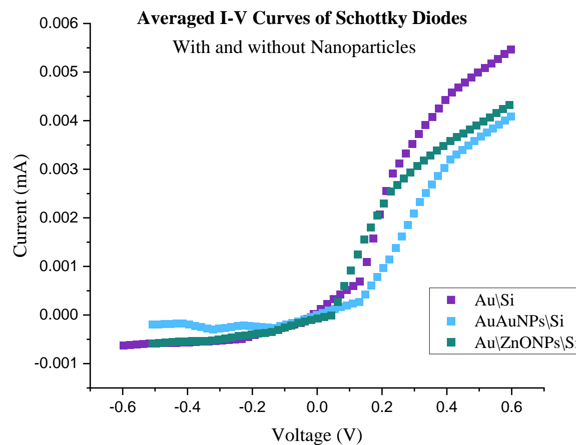

Fig. (4.22): Averaged I-V curves of Au\Si Schottky diodes with and without particles

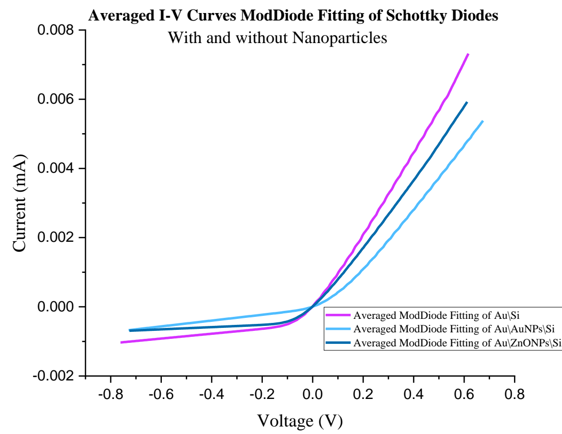

Fig. (4.23): Averaged ModDiode fitting of the set with gold and metallised layer, with and without the nanoparticles.

However, the barrier height yielded a negative value which may be an indication to an ohmic contact, this may be due to the contact point on the diode; where an error with the high thickness of silver paint used to create the contact point with the diode and the micromanipulators, again, causing a possible overlap in the roles of the metallised layer of gold, and the inserted silver paint on the top.

This concludes the results and discussion, next, the work in this study is to be concluded with a possible recommendation for future work.

Chapter 5: Conclusion and Future work

Two different structures of the metal-insulator-semiconductor Schottky diodes has been successfully fabricated in the laboratory. Both silver and gold were evaporated as the metal layer of the junction, whereas for the interface layer, gold (Au) nanoparticles, 10nm in diameter, and Zinc oxide (ZnO) nanoparticles, with less that 100nm in diameter, were selected. The formation procedure of Schottky diodes involves several steps: chemical etching of Si substrates, spin-coating of NPs on the substrate and metal evaporation in vacuum onto the modified Si substrates. Prior to the metal deposition, the embedding of the nanoparticles was verified with FTIR spectroscopy. The surface monitoring and the electrical characterisation of the assembled Schottky diode were carried out using the current-voltage measurements.

Etching with KOH showed a successful cleaning of the Si substrate surface which was tested by the contact angle measurements. Then, the spin-coating technique performed to uniformly spread the nanoparticles layer on each designated Si substrate, which was proved to be successful by the results of the FTIR. Moreover, the evaporation of silver and gold was well executed in vacuum using the bell jar.

Furthermore, the pieced Schottky diodes were categorised in groups, each group containing three types of samples according to the particles present at the junction; the first type is with no added NPs at the junction, the second type is with AuNPs, and the last with ZnONPs. Each sample was placed in a circuit using micromanipulators with bias voltage in order to obtain its I-V characterisation. In addition, the silver-nanoparticles-silicon samples electrical behavior was efficiently investigated under light illumination.

Results showed an improved electrical behavior of the Schottky diode after inserting the nanoparticles at the junction, which was mainly noted in the decreased values of the barrier height in the presence of NPs. Series and shunt resistances were monitored as important parameters that could be affected by the presence of nanoparticles. An increase in series and

shunt resistances has been observed, while a decreased value of these resistances was observed upon illumination of Schottky devices with nanoparticles.

However, there has been some limitations to our study that affected some of the results. The fabrication of an ideal Schottky diode involves a well-advanced technology, in addition to the required working hours to characterise the related apparatus. The laboratory where this study took place has limited options and potentials, however, we were able to construct the desired Schottky diode with its primal components successfully enough to note the slightest effect caused by the addition of the NPs to the junction.

Appendix 1 shows the standard deviation taken for some samples, concerning the parameters I_o, R_s, R_{sh}, and Φ_b, it is noted that the value of the standard deviation is significantly high, this might have resulted from many factors in our experiment.

The error may have been a result of the micromanipulators, and how far they might have sunk into the fabricated diode, caused by scratches on the metalized layer, moreover, the needles of the micromanipulators may have not been adjusted equally every time. This indicated the high sensitivity of the fabricated diodes.

Another possible cause of the high resistance is the thickness of the silver paint used to create the contact points with the micromanipulators, causing the diode’s behavior to be more like with ohmic resistance. Moreover, the distance between the two silver paint points created on the fabricated Schottky diode may have cause extra resistance.

This experiment showed the significance of the etching procedure, though etching with KOH needs an enhancement to prevent any oxidation of the Si substrate, which may be achieved with the Nitrogen gas bath of the samples.

Finally, the addition of the nanoparticles showed promising results to consider further investigation on their effect on the electronic and optoelectronic devices. Also, the time sensitivity of the samples implies the importance of fast machinery intervention in the advanced studies, especially in the diode fabrication steps. The need to improve these electronics requires a thorough investigation of the fabricated Schottky diodes with the addition of nanoparticles with suitable characterization apparatus.

References

Aazou, S., & Assaid, E. M. (2010). *Schottky diode parameters extraction using two different methods*. https://doi.org/10.1109/ICM.2009.5418642

Abbas, Y., Rezk, A., Anwer, S., Saadat, I., Nayfeh, A., & Rezeq, M. d. (2020). Improved figures of merit of nano-Schottky diode by embedding and characterizing individual gold nanoparticles on n-Si substrates. *Nanotechnology*, *31*(12), 125708.

Ajadi, D., Agboola, S., & Adedokun, O. (2016). Effect of Spin Coating Speed on Some Optical Properties of ZnO Thin Films. *Journal of Materials Science and Chemical Engineering*, *04*, 1-6. https://doi.org/10.4236/msce.2016.45001

Allsopp, M. (2007). Nanotechnologies and nanomaterials in electrical and electronic goods: A review of uses and health concerns.

Angermann, H., Henrion, W., Röseler, A., & Rebien, M. (2000). Wet-chemical passivation of Si(111)- and Si(100)-substrates. *Materials Science and Engineering: B*, *73*, 178–183. https://doi.org/10.1016/S0921-5107(99)00457-2

AnoopPrakashA, B., Jency, J. G., & Mathew, M. C. (2013). A Review of various Wet Etching Techniques used in Micro Fabrication for Real Estate Consumption.

Arizumi, T., Hirose, M., & Altaf, N. (1968). Au-Ag Alloy-Silicon Schottky Barriers. *Japanese Journal of Applied Physics*, *7*(8), 870-874. https://doi.org/10.1143/jjap.7.870

Boutelala, A., Bourfa, F., & Mahtali, M. (2020). Effect of light on electrical and photoelectrical characteristics of Al/TiO2/p-Si Schottky diode. *Journal of Materials Science: Materials in Electronics*, *31*(14), 11379-11389. https://doi.org/10.1007/s10854-020-03687-y

Boylestad, R. L. N. L. (2013). *Electronic devices and circuit theory*. Pearson Prentice Hall.

Das, M., Das, P., Datta, J., Das, D., Acharya, S., & Ray, P. P. (2021). Improved device performance of rod like ZnO in a Schottky type photosensor compared to particle like ZnO: Analysis of charge transport. *Materials Science in Semiconductor Processing*, *130*, 105799. https://doi.org/https://doi.org/10.1016/j.mssp.2021.105799

Doyle, W. M. (2017). Principles and Applications of Fourier Transform Infra-red (FTIR) Process Analysis.

Dutka, M. V. (2014). Processing and structure of nanoparticles.

Feynman, R. P. (1992). There's plenty of room at the bottom [data storage]. *Journal of Microelectromechanical Systems*, *1*(1), 60-66. https://doi.org/10.1109/84.128057

Foo, K. L., Kashif, M., & Hashim, U. (2013). Study of Zinc Oxide Films on SiO₂/Si Substrate by Sol–Gel Spin Coating Method for pH Measurement. *Applied Mechanics and Materials*, *284*, 347-351. https://doi.org/10.4028/www.scientific.net/AMM.284-287.347

Franssila, S. (2010). Introduction to microfabrication, second edition. http://www.books24x7.com/marc.asp?bookid=43226

Ghabboun, J. (2004). *Making Molecularly Modified Devices: The Importance of Contact Deposition for Semiconductor/Molecules/Metal Junction Properties* Rehovot, Israel.

Gholami, S., Khakbaz, M. J. W. A. o. S., Engineering, Technology, I. J. o. E., Computer, Energetic, Electronic, & Engineering, C. (2011). Measurement of I-V Characteristics of a PtSi/p-Si Schottky Barrier Diode at low Temperatures. *5*, 1285-1288.

Gorji, M. S., Razak, K. A., & Cheong, K. Y. (2015). Schottky barrier height engineering of Al contacts on Si by embedded Au nanoparticles. *Microelectronic Engineering*, *133*, 110-119. https://doi.org/https://doi.org/10.1016/j.mee.2014.11.007

Griffiths, P. R. D. H. J. A. (2007). *Fourier transform infrared spectrometry*. Wiley-Interscience.

Gurunathan, S., Han, J., Park, J., & Kim, J.-H. (2014). Green chemistry approach for synthesizing biocompatible gold nanoparticles. *Nanoscale Research Letters*, *9*, 248. https://doi.org/10.1186/1556-276X-9-248

Herizchi, R., Abbasi, E., Milani, M., & Akbarzadeh, A. (2016). Current methods for synthesis of gold nanoparticles. *Artificial Cells, Nanomedicine, and Biotechnology*, *44*(2), 596-602. https://doi.org/10.3109/21691401.2014.971807

Hoseinpour, V., Souri, M., Ghaemi, N., & Shakeri, A. (2017). Optimization of green synthesis of ZnO nanoparticles by Dittrichia graveolens (L.) aqueous extract. *1*, 39-49. https://doi.org/10.22034/HBB.2017.10

HU, C. (2010). *Modern semiconductor devices for integrated circuits*. Pearson Education.

Janotti, A., & Van de Walle, C. (2009). Fundamentals of Zinc Oxide As a Semiconductor. *Reports on Progress in Physics*, *72*, 126501. https://doi.org/10.1088/0034-4885/72/12/126501

Jayarambabu, N., Kumari, Rao, K., & Prabhu, Y. (2015). BENEFICIAL ROLE OF ZINC OXIDE NANOPARTICLES ON GREEN CROP PRODUCTION. *INTERNATIONAL JOURNAL OF MULTIDISCIPLINARY ADVANCED RESEARCH TRENDS*, *2*, 2349-7408.

Kaufmann, I. R., Zerey, O., Meyers, T., Reker, J., Vidor, F., & Hilleringmann, U. (2021). A Study about Schottky Barrier Height and Ideality Factor in Thin Film Transistors with Metal/Zinc Oxide Nanoparticles Structures Aiming Flexible Electronics Application. *Nanomaterials*, *11*(5), 1188. https://www.mdpi.com/2079-4991/11/5/1188

Khan, I., Saeed, K., & Khan, I. (2019). Nanoparticles: Properties, applications and toxicities. *Arabian Journal of Chemistry*, *12*(7), 908-931. https://doi.org/https://doi.org/10.1016/j.arabjc.2017.05.011

Kittel, C. (2005). *Introduction to Solid State Physics* (8 ed.). John Wiley & Sons, Inc.

Kumbhakar, P., Ray, S. S., & Stepanov, A. L. (2014). Optical Properties of Nanoparticles and Nanocomposites. *Journal of Nanomaterials*, *2014*, 181365. https://doi.org/10.1155/2014/181365

Labar, R., & Kundu, T. K. (2022). Fabrication and Characterization of Back-to-Back Schottky Diode in Ni/ZnO/Ag Nanojunction. *Journal of Electronic Materials*, *51*(1), 223-231. https://doi.org/10.1007/s11664-021-09280-1

Liau, L. C.-K., & Lin, Y.-H. (2017). Effects of electric fields on the conduction of polyvinyl alcohol (PVA)/ZnO films by photoluminescence analysis. *Journal of Luminescence*, *181*(C), 217-222. https://doi.org/10.1016/j.jlumin.2016.08.067

Lorenz-Fonfria, V. A. (2020). Infrared Difference Spectroscopy of Proteins: From Bands to Bonds. *Chemical Reviews*, *120*(7), 3466-3576. https://doi.org/10.1021/acs.chemrev.9b00449

Martín-Palma, R. J., & Lakhtakia, A. (2013). Chapter 15 - Vapor-Deposition Techniques. In A. Lakhtakia & R. J. Martín-Palma (Eds.), *Engineered Biomimicry* (pp. 383-398). Elsevier. https://doi.org/https://doi.org/10.1016/B978-0-12-415995-2.00015-5

Mater, A., Lett, Bhau, B., Ghosh, S., Puri, S., Borah, B., Sarmah, D., & Khan, R. (2015). Green Synthesis Of Gold Nanoparticles From The Leaf Extract Of Nepenthes Khasiana And Antimicrobial Assay. *Advance Material Letters*, *6*, 55-58. https://doi.org/10.5185/amlett.2015.5609

Mishra, U., & Singh, J. (2007). *Semiconductor Device Physics and Design*. Springer Netherlands. https://books.google.ps/books?id=7WKOfUR-8M4C

Mohan, J., G, P., Chennazhi, K., Jayakumar, R., & Nair, S. (2013). Functionalised gold nanoparticles for selective induction of in vitro apoptosis among human cancer cell lines. *Journal of Experimental Nanoscience - J EXP NANOSCI*, *8*, 32-45. https://doi.org/10.1080/17458080.2011.557841

Neikov, O. D., & Yefimov, N. A. (2019). Chapter 9 - Nanopowders. In O. D. Neikov, S. S. Naboychenko, & N. A. Yefimov (Eds.), *Handbook of Non-Ferrous Metal Powders (Second Edition)* (pp. 271-311). Elsevier. https://doi.org/https://doi.org/10.1016/B978-0-08-100543-9.00009-9

O.K, S., Nair, P., & Anuradha.M.Ashok. (2018). Engineered nanomaterials for energy applications-“Nanomaterials for Solar Energy Generation”-Handbook of Nanomaterials for Engineering Applications. In (pp. 751-767). https://doi.org/10.1016/B978-0-12-813351-4.00043-2

Pal, P., & Singh, S. S. (2013). A New Model for the Etching Characteristics of Corners Formed by Si{111} Planes on Si{110} Wafer Surface. *Engineering*, *2013*, 1-8.

Petty, M. C. (2007). *Molecular Electronics: From Principles to Practice* (1 ed.). John Wiley & Sons Ltd.

Pierret, R. F. (2006). *Semiconductor device fundamentals*. Addison-Wesley Longman.

Ramadan, R., & Martín-Palma, R. J. (2020). Electrical Characterization of MIS Schottky Barrier Diodes Based on Nanostructured Porous Silicon and Silver Nanoparticles with Applications in Solar Cells. *Energies*, *13*(9), 2165. https://www.mdpi.com/1996-1073/13/9/2165

Rouis, A., Hizem, N., Hassen, M., & Kalboussi, A. (2021). Electrical Properties of Silicon Nanowires Schottky Barriers Prepared by MACE at Different Etching Time. *Silicon*. https://doi.org/10.1007/s12633-021-01261-7

Sahu, N., Parija, B., & Panigrahi, S. (2009). Fundamental understanding and modeling of spin coating process: A review. *Indian Journal of Physics*, *83*(4), 493-502. https://doi.org/10.1007/s12648-009-0009-z

Sathyanarayana, D. N. (2004). Vibrational spectroscopy : theory and applications / D.N. Sathyanarayana.

Society, R., & Engineering, R. A. o. (2004). *Nanoscience and Nanotechnologies: Opportunities and Uncertainties*. Royal Society. https://books.google.ps/books?id=D-m_SgAACAAJ

Song, X., Han, B., Yu, X., & Hu, W. (2020). The analysis of charge transport mechanism in molecular junctions based on current-voltage characteristics. *Chemical Physics*, *528*, 110514. https://doi.org/https://doi.org/10.1016/j.chemphys.2019.110514

Sousa, L. M., Vilarinho, L. M., Ribeiro, G. H., Bogado, A. L., & Dinelli, L. R. (2017). An electronic device based on gold nanoparticles and tetraruthenated porphyrin as an electrochemical sensor for catechol. *Royal Society open science*, *4*(12), 170675-170675. https://doi.org/10.1098/rsos.170675

Subara, D., & Jaswir, I. (2018). Gold Nanoparticles: Synthesis and application for Halal Authentication in Meat and Meat Products. *8 (2018)*. https://doi.org/10.18517/ijaseit.8.4-2.7055

Subedi, D. P. (2011). Contact Angle Measurement for The Surface Characterization of Solids. *Himalayan Physics*, *2*(2), 1-4. https://doi.org/10.3126/hj.v2i2.5201

Sze, S. M. (1994). *Semiconductor Sensors*. Wiley. https://books.google.ps/books?id=hoBRAAAAMAAJ

Sze, S. M. (2002). *Semiconductor devices, physics and technology* (2 ed.). John Wiley & Sons, Inc.

Tong, N. T., & Pora, W. (2016). A parameter extraction technique exploiting intrinsic properties of solar cells. *Applied Energy*, *176*, 104-115. https://doi.org/https://doi.org/10.1016/j.apenergy.2016.05.064

Vilan, A., & Cahen, D. (2017). Chemical Modification of Semiconductor Surfaces for Molecular Electronics. *Chemical Reviews*, *117*(5), 4624-4666. https://doi.org/10.1021/acs.chemrev.6b00746

Wang, C., Kim, J., Jin, C., Leong, P., & McEwan, A. (2012). Review: Near infrared spectroscopy in optical coherence tomography. *Journal of Near Infrared Spectroscopy*, *20*, 237. https://doi.org/10.1255/jnirs.975

Wang, Y. (2016). Koh etching of silicon.

Whatmore, R. W. (2006). Nanotechnology—what is it? Should we be worried? *Occupational Medicine*, *56*(5), 295-299. https://doi.org/10.1093/occmed/kql050

Wilson, K. W. J. M. H. A. C. S. (2018). *Wilson and Walker's principles and techniques of biochemistry and molecular biology*.

Xiong, G., Pal, U., Serrano, J. G., Ucer, K. B., & Williams, R. T. (2006). Photoluminesence and FTIR study of ZnO nanoparticles: the impurity and defect perspective. *physica status solidi c*, *3*(10), 3577-3581. https://doi.org/https://doi.org/10.1002/pssc.200672164

Yilbas, B. S., Al-Sharafi, A., & Ali, H. (2019). Chapter 3 - Surfaces for Self-Cleaning. In B. S. Yilbas, A. Al-Sharafi, & H. Ali (Eds.), *Self-Cleaning of Surfaces and Water Droplet Mobility* (pp. 45-98). Elsevier. https://doi.org/https://doi.org/10.1016/B978-0-12-814776-4.00003-3

APPENDIX 1

The importance of calculating the standard deviation is knowing the reliability of the data obtained from the experiment, allowing further interpretation and noting errors to be taken into consideration in future work. This experiment has showed a high standard deviation concerning the series and shunt resistances showed in the following tables:

Table A.1 Standard deviation Ag\Si Dark

Samples of Ag\Si	I_o (A)	R_s (Ω)	R_{sh} (Ω)	Φ_b(V)
1	3.41E-11	117.9979	3562.653	0.29
2	1.37E-10	121.3147	5084.695	0.36
3	6.84E-19	22.70616	1385.752	0.78
4	1.44E-08	177.3851	6228.163	0.34
5	4.38E-07	169.7366	12315.09	0.19
6	1.12E-07	163.2478	31168.18	0.29
7	4.40E-07	1.70E+02	1.23E+04	0.209
8	1.20E-08	152.5766	19786.9	0.268
9	4.11E-09	150.663	20430.45	0.4
Standard Deviation	1.88E-07	48.15779	9761.418	0.175694

Table A.2: Standard deviation Ag\Si Light

Samples of Ag\Si	I_o (A)	R_s (Ω)	R_{sh} (Ω)	Φ_b(V)
1	2.32E-08	1767.272	83286.79	0.14
2	9.96E-10	1825.812	25454.52	0.11
3	1.04E-09	1813.897	25425.01	0.15
Standard Deviation	1.28171E-08	30.93769	33398	0.020817

Table A.3: Standard deviation Ag\AuNPs\Si Dark

Samples of Ag\AuNPs\Si	I_o (A)	R_s (Ω)	R_{sh} (Ω)	Φ_b(V)
1	5.85E-07	357.0064	4053.681	0.28
2	8.39E-08	140.9144	7583.188	0.33
3	8.55E-06	134.2156	3158.263	0.15
4	1.78E-09	59.10517	11796.29	0.27
5	2.06E-06	118.7482	515.0324	0.26
6	2.79E-06	125.7914	4325.174	0.12
7	4.58E-07	157.3519	4.81E+03	0.14
Standard Deviation	3.04085E-06	93.80494	3594.856	0.08275

Table A.4: Standard deviation Ag\AuNPs\Si Light

Samples of Ag\AuNPs\Si	I_o (A)	R_s (Ω)	R_{sh} (Ω)	Φ_b(V)
1	2.37E-04	1.28426	36.33793	0.04
2	2.45E-04	1.2831	36.78633	0.15
3	2.82E-04	1.28918	36.82007	0.06
4	4.42E-04	1.30022	37.25756	0.11
5	2.08E-04	0.94865	8.71415	0.098
6	6.65E-04	1.66941	27.22252	0.11
Standard Deviation	0.000177	0.228235	11.35402	0.039328

Table A.5: Standard deviation Ag\ZnONPs\Si Dark

Samples of Ag\ZnONPs\Si	I_o (A)	R_s (Ω)	R_{sh} (Ω)	Φ_b(V)
1	1.67E-10	89.52317	53218.92	0.28
2	6.15E-06	127.4919	6575.866	0.155
3	1.82E-09	134.4626	1471.722	0.14
4	3.16E-08	144.4012	2590.482	0.2
5	1.63E-07	141.2406	4023.086	0.18
Standard Deviation	2.72832E-06	22.16496	22243.07	0.054818

Table A.6: Standard deviation Ag\ZnONPs\Si Light

Samples of Ag\ZnONPs\Si	I_o (A)	R_s (Ω)	R_{sh} (Ω)	Φ_b(V)
1	9.25E-07	3.33313	66.55105	0.06
2	8.55E-07	3.33566	47.30249	0.109
3	1.01E-06	3.36211	46.52983	0.09
4	7.63E-07	3.30475	48.12718	0.09
5	1.58E-05	1.5	21.07155	0.07
6	2.94E-06	2.58653	33.15897	0.108
7	2.82E-07	1.45	23.50882	0.23
Standard Deviation	5.59363E-06	0.878049	16.0127	0.056688